

# Chemistry—A European Journal

## Supporting Information

### Insights into LiAlH<sub>4</sub> Catalyzed Imine Hydrogenation

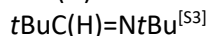
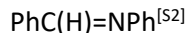
Holger Elsen, Jens Langer, Gerd Ballmann, Michael Wiesinger, and Sjoerd Harder\*<sup>[a]</sup>

## **Table of contents**

General.....	S2
NMR-Spectra.....	S3
Crystallographic Information.....	S23
DFT Calculations.....	S34
References.....	S59

## General

All experiments were carried out in dry glassware under N<sub>2</sub> using standard Schlenk techniques and freshly dried and degassed solvents (all solvents were dried over a column except for THF which was dried over Na-benzophenone and redistilled). Commercially available LiAlH<sub>4</sub> was extracted with diethyl ether and after removal of all solvents dried in vacuo to give a white fluffy material. Commercially available NaAlH<sub>4</sub> was purified via a similar method using THF·KAlH<sub>4</sub>·[18-crown-6/THF] was prepared according to Trzaska.<sup>[S1]</sup> Ph(H)C=NtBu was obtained commercially from Sigma-Aldrich, 97 %. Following imine substrates were prepared according to literature procedures:



Hydrogen of quality N5 has been used for catalytic hydrogenation. Deuterated solvents were dried over molsieves (3 Å) in a glovebox. All substrates were dried by stirring over freshly powdered CaH<sub>2</sub> at 60 °C. Reactors were dried by heating overnight in an oven at 70 °C. The products of catalysis have been analyzed by NMR. Conversions were determined by integration of characteristic signals.

NMR spectra were measured on Bruker Avance III HD 400 MHz and Bruker Avance III HD 600 MHz spectrometers. Elemental analysis was performed with an Hekatech Eurovector EA3000 analyzer. Crystal structures have been measured on a SuperNova (Agilent) diffractometer with dual Cu and Mo microfocus sources and an Atlas S2 detector. Crystallographic data have been deposited with the Cambridge Crystallographic Data Centre as supplementary publication 2024356-2024363.

## NMR-Spectra

### Reference Spectra

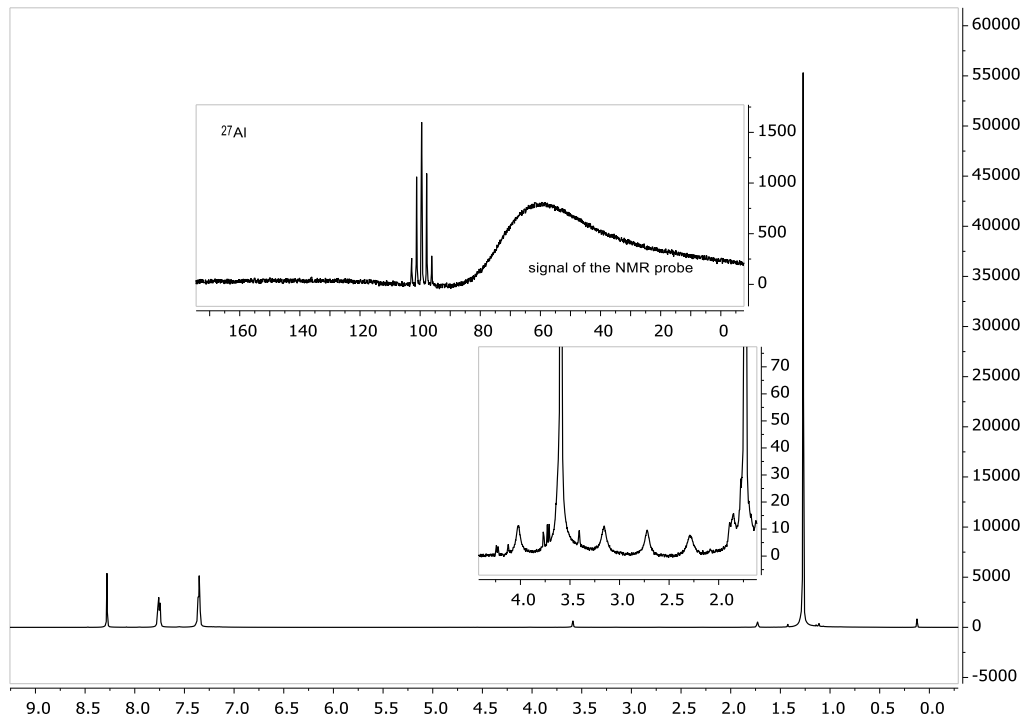


Figure S1: Reference spectra of  $\text{KAlH}_4$  produced by the reaction of  $\text{KH}$  with  $\text{AlH}_3\text{THF}_2$  in pure  $\text{PhC}(\text{H})=\text{NtBu}$  (no-D-NMR).

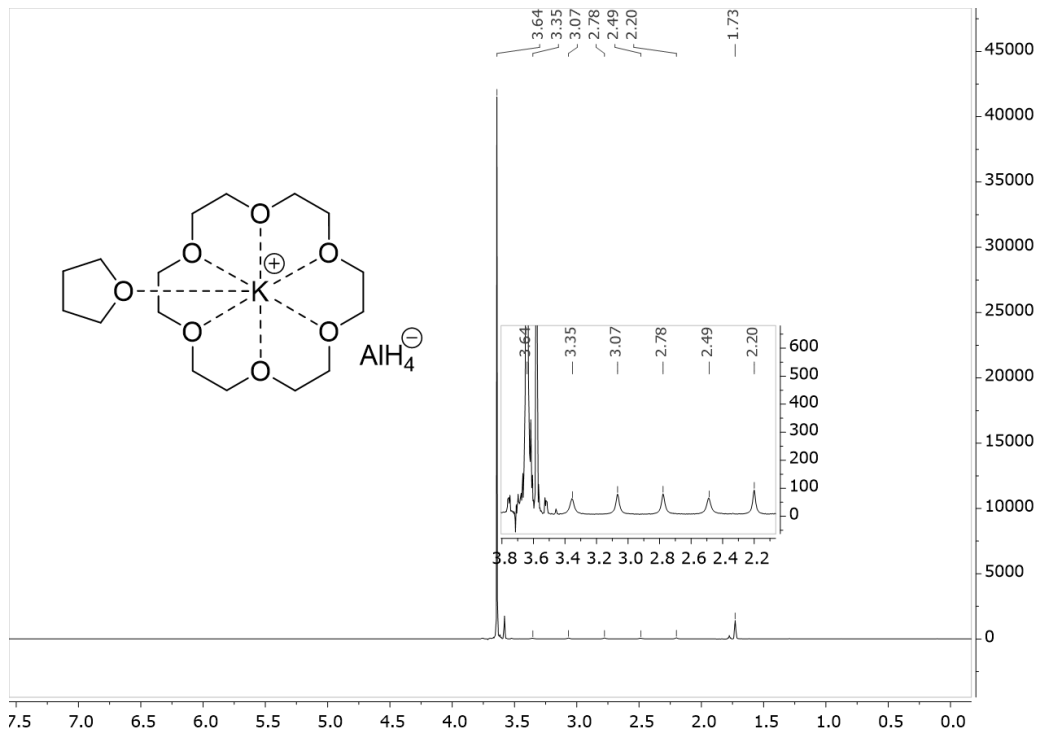


Figure S2: Reference  $^1\text{H}$ -NMR of  $\text{KAlH}_4 \cdot [18\text{-crown-6}/\text{THF}]$  in  $\text{THF}-d_8$ .

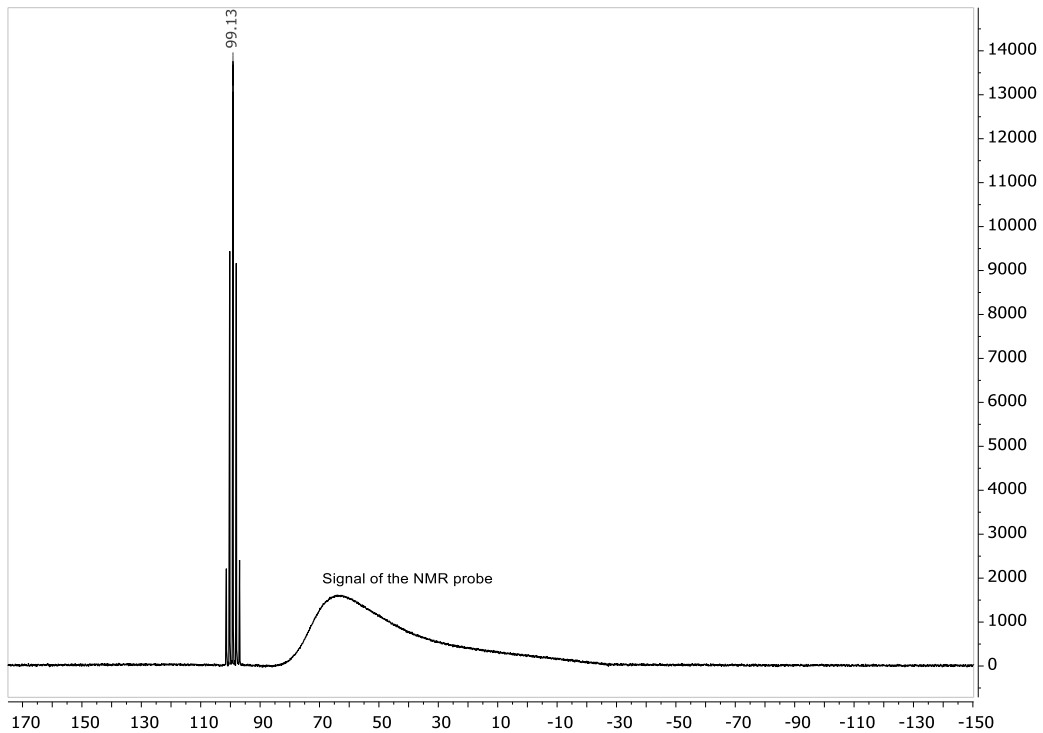


Figure S3: Reference  $^{27}\text{Al}$ -NMR of  $\text{KAlH}_4 \cdot [18\text{-crown-6}/\text{THF}-d_8]$ .

### Catalytic reductions

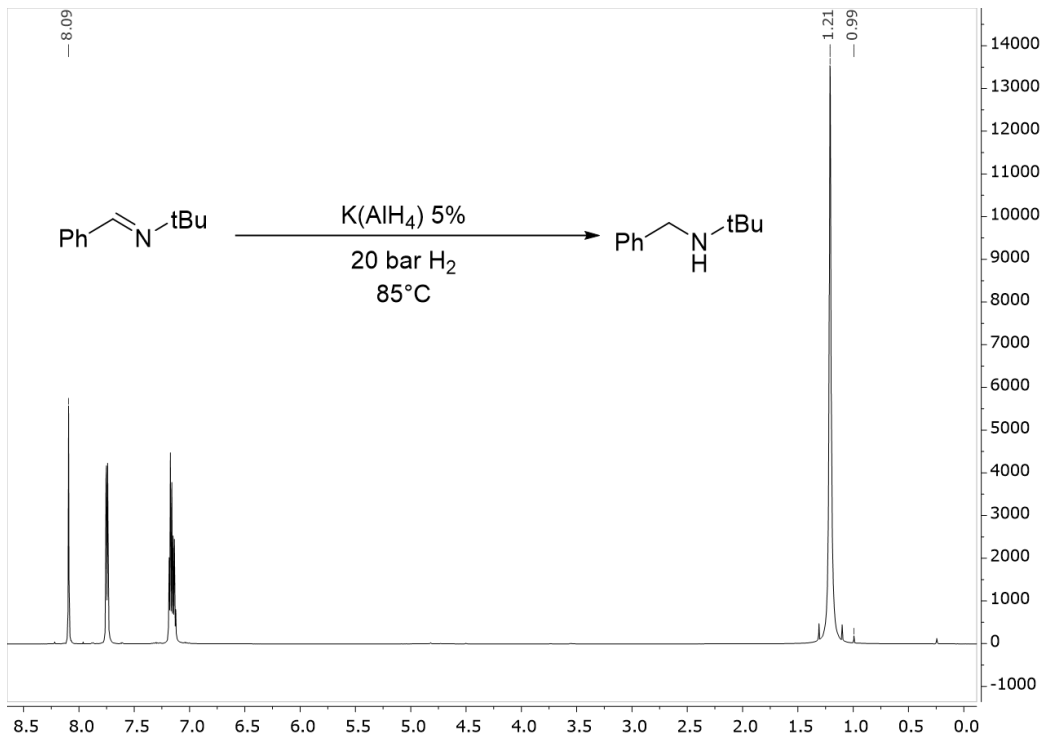


Figure S4: Catalytic reduction of  $\text{PhC}(\text{H})=\text{N}-\text{tBu}$  using 5 mol%  $\text{KAlH}_4$  at 20 bar  $\text{H}_2$  and  $85^\circ\text{C}$  in neat imine after 24h. NMR in  $\text{C}_6\text{D}_6$ .

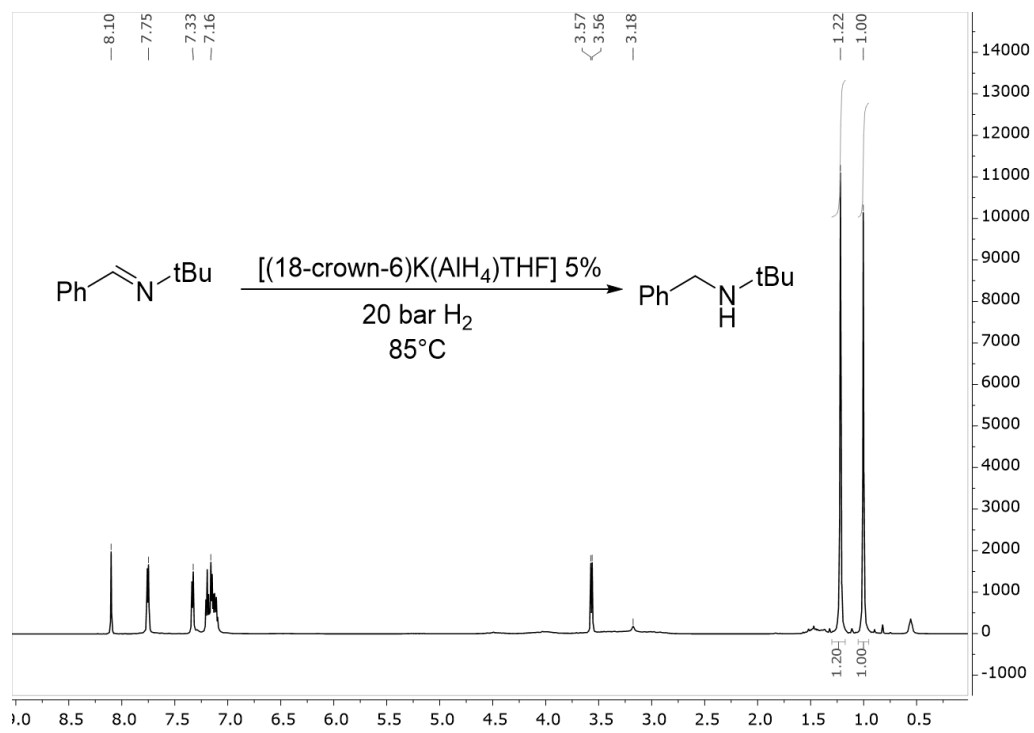


Figure S5: Catalytic reduction of  $\text{PhC}(\text{H})=\text{NtBu}$  using 5 mol%  $[(18\text{-crown-6})\text{K}(\text{AlH}_4)\text{THF}]$  at 20 bar  $\text{H}_2$  and 85°C in neat imine after 24h. NMR in  $\text{C}_6\text{D}_6$ .

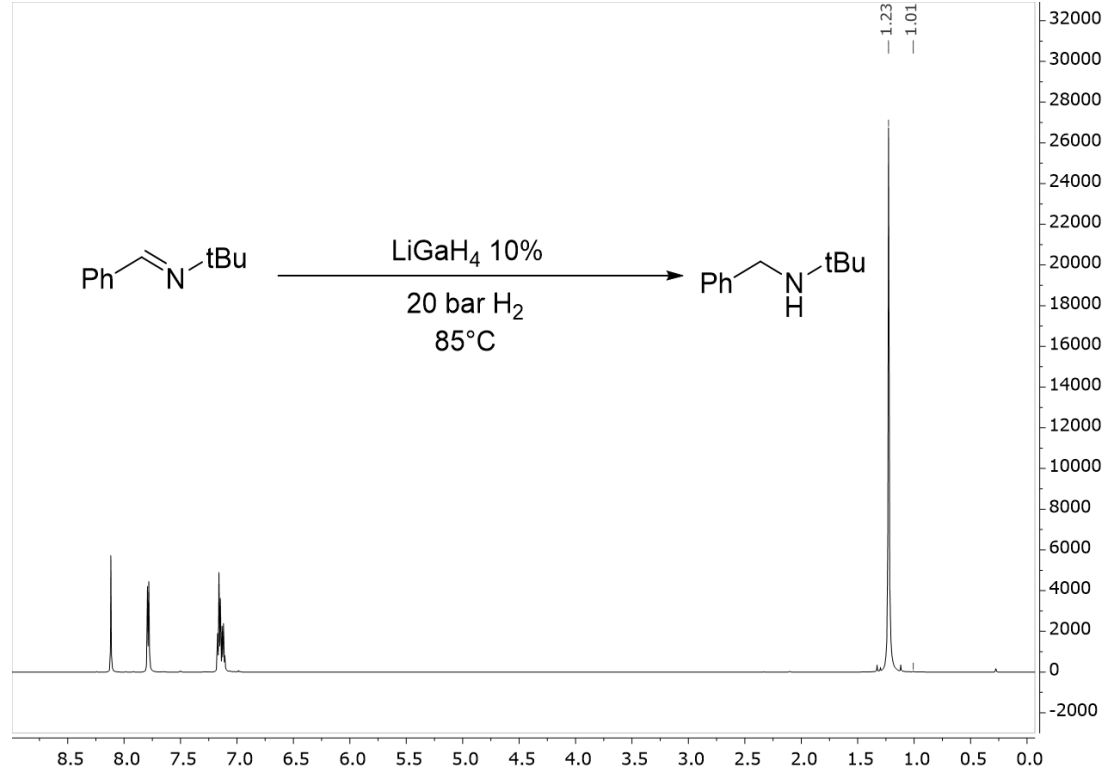


Figure S6: Catalytic reduction of  $\text{PhC}(\text{H})=\text{NtBu}$  using 10 mol%  $\text{LiGaH}_4\cdot(\text{TMEDA})_2$  at 20 bar  $\text{H}_2$  and 85°C in neat imine after 24h. NMR in  $\text{C}_6\text{D}_6$ .

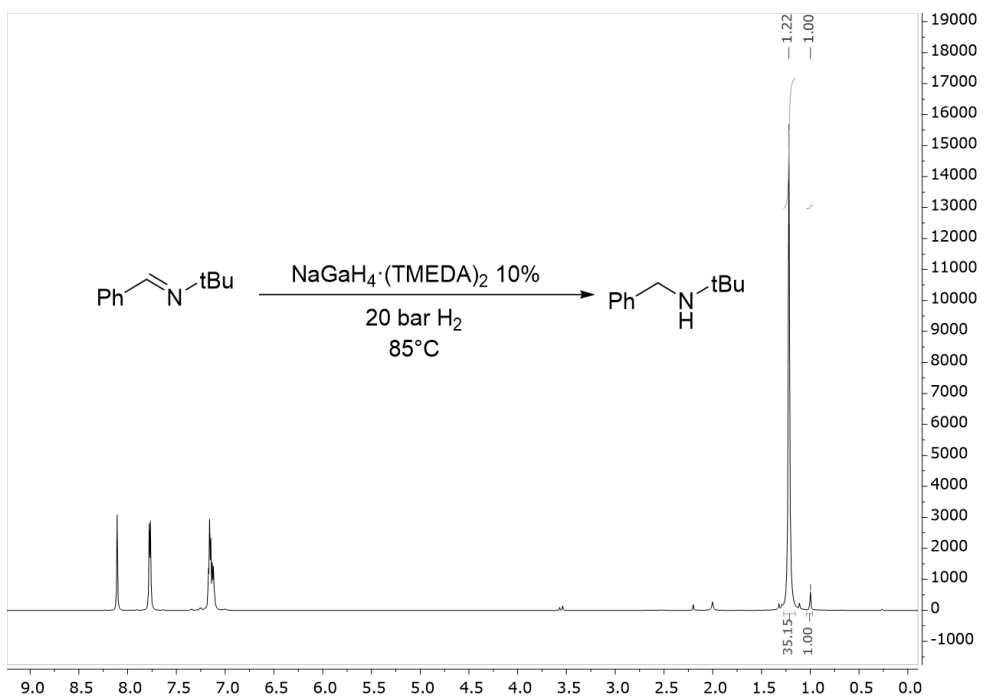


Figure S7: Catalytic reduction of  $\text{PhC}(\text{H})=\text{NtBu}$  using 10 mol%  $\text{NaGaH}_4\cdot(\text{TMEDA})_2$  at 20 bar  $\text{H}_2$  and  $85^\circ\text{C}$  in neat imine after 24h. NMR in  $\text{C}_6\text{D}_6$ .

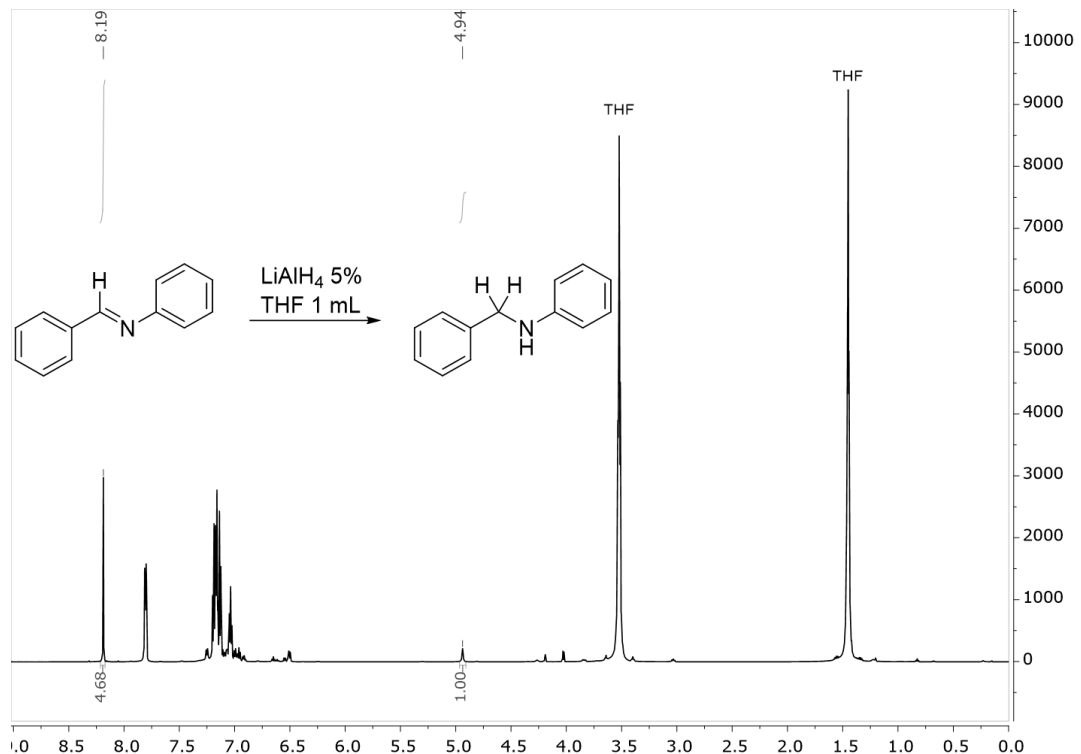


Figure S8:  $^1\text{H-NMR}$  of the reduction of  $\text{PhC}(\text{H})=\text{NPh}$  imine with  $\text{LiAlH}_4$  (5mol%) at  $85^\circ\text{C}$  under 20 atm.  $\text{H}_2$  after 4 days. NMR in  $\text{C}_6\text{D}_6$

## Complex Spectra

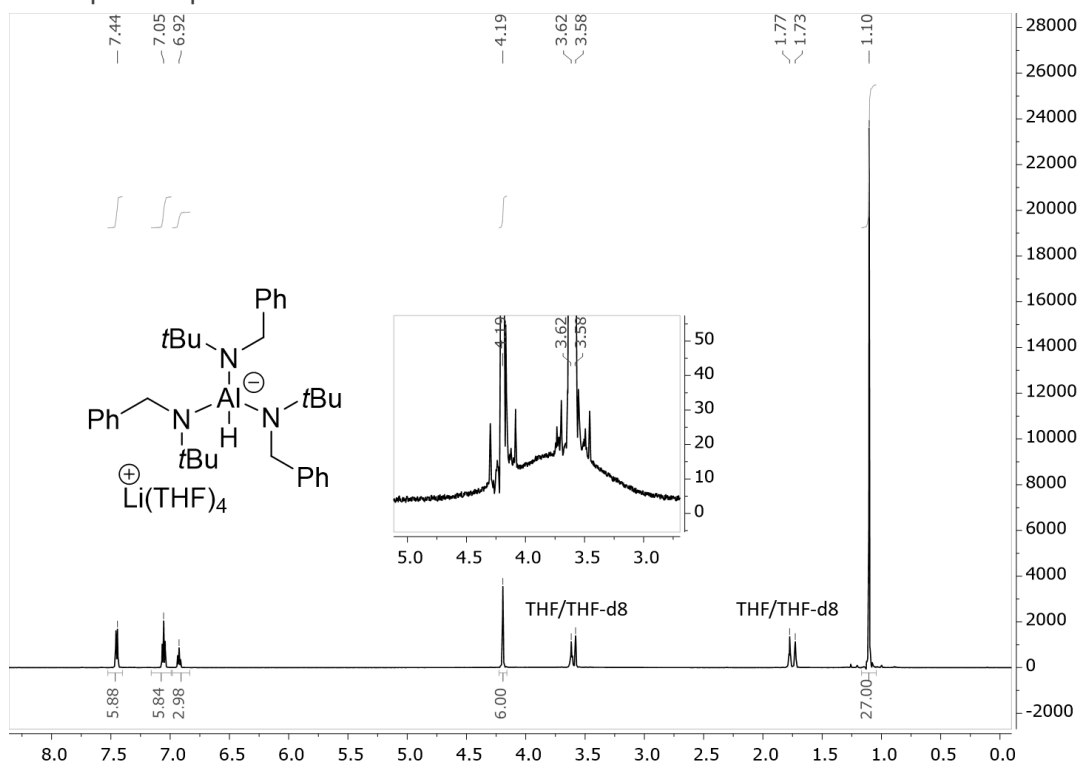


Figure S9:  $^1\text{H}$ -NMR of  $\text{LiAlH}[\text{N}(\text{tBu})\text{CH}_2\text{Ph}]_3 \cdot (\text{THF})_4$  (**1**). NMR in  $\text{THF}-d_8$ .

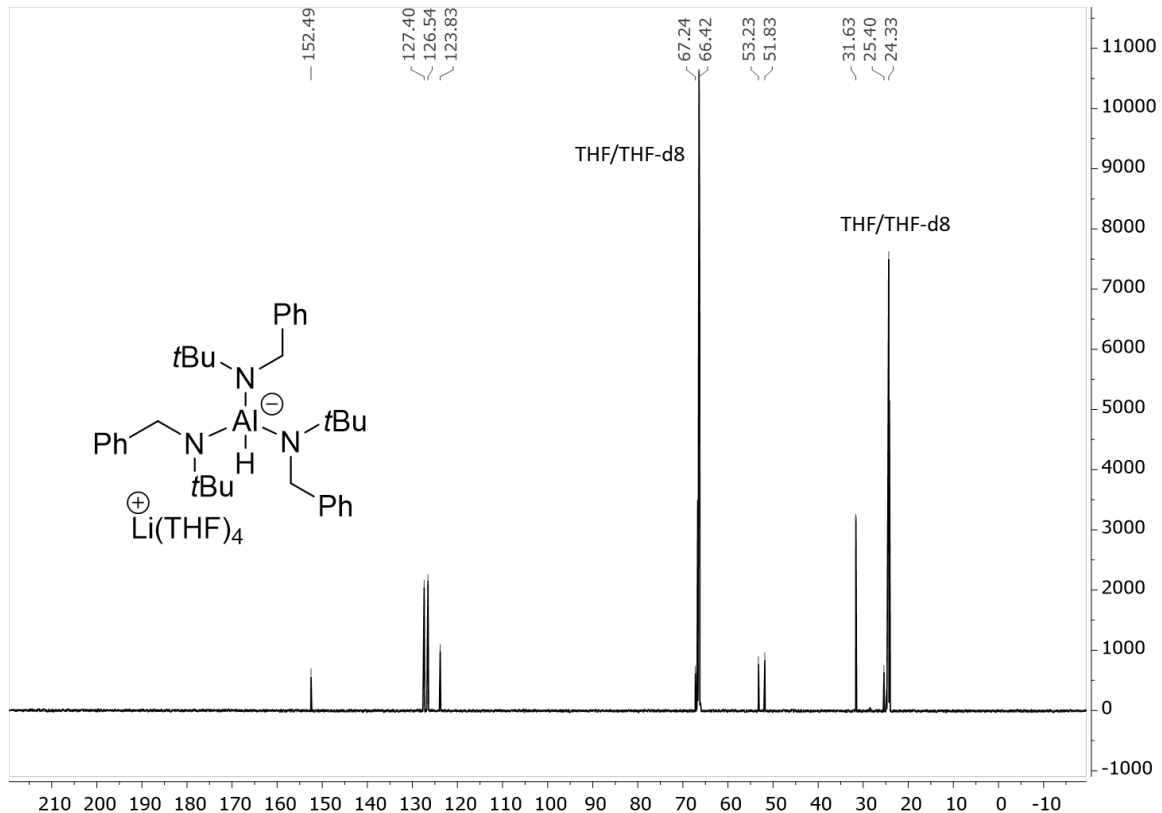


Figure S10:  $^{13}\text{C}$ -NMR of  $\text{LiAlH}[\text{N}(\text{tBu})\text{CH}_2\text{Ph}]_3 \cdot (\text{THF})_4$  (**1**). NMR in  $\text{THF}-d_8$ .

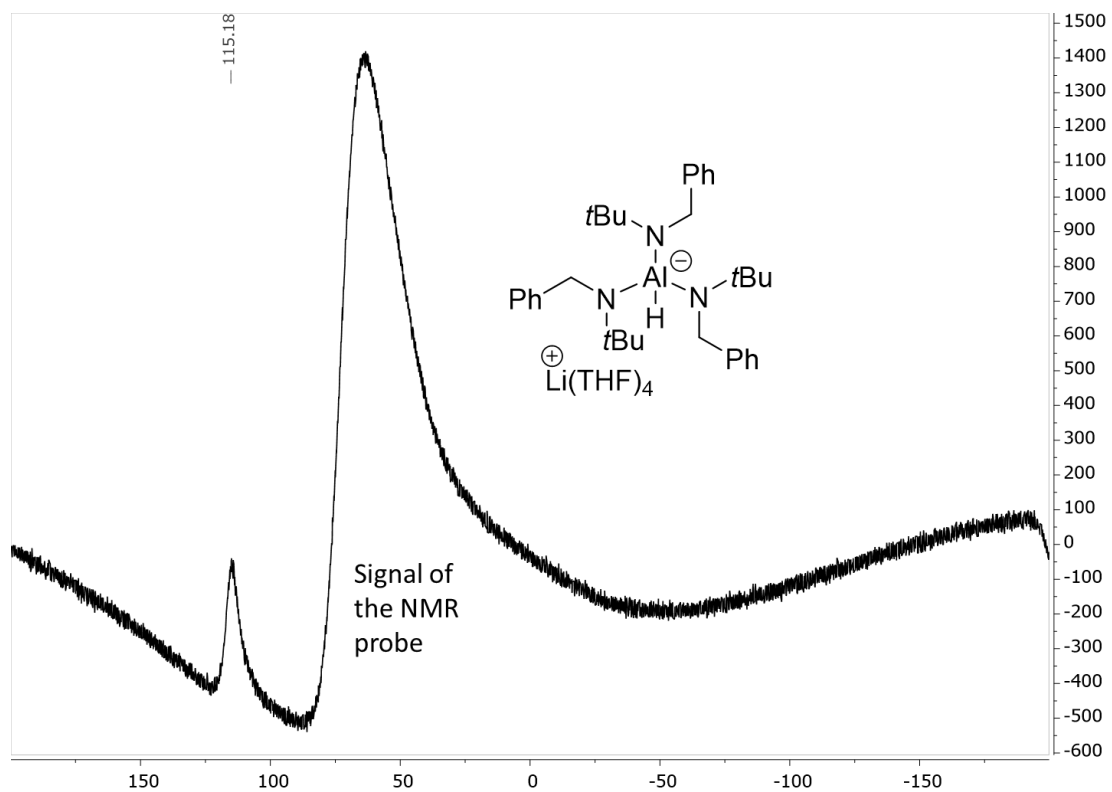


Figure S11:  $^{27}\text{Al}$ -NMR of  $\text{LiAlH}[\text{N}(t\text{Bu})\text{CH}_2\text{Ph}]_3 \cdot (\text{THF})_4$  (**1**). NMR in  $\text{THF}-d_8$ .

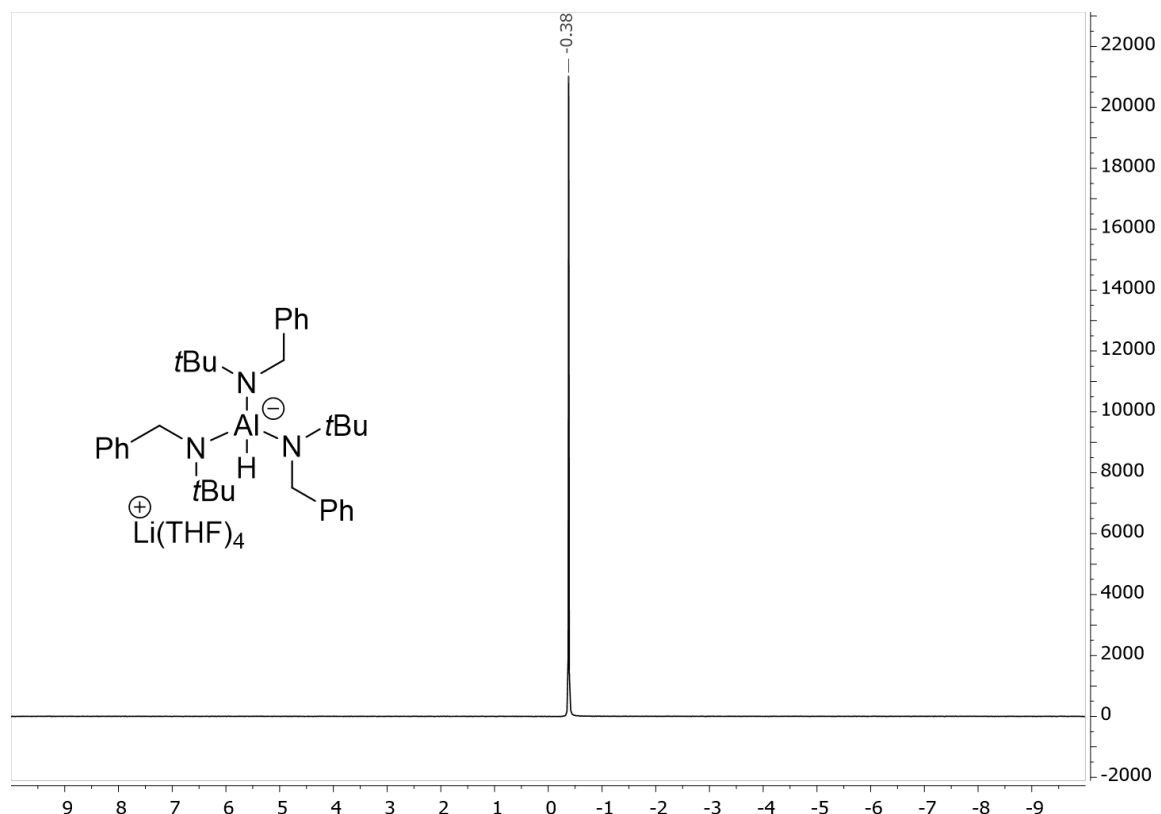


Figure S12:  $^7\text{Li}$ -NMR of  $\text{LiAlH}[\text{N}(t\text{Bu})\text{CH}_2\text{Ph}]_3 \cdot (\text{THF})_4$  (**1**). NMR in  $\text{THF}-d_8$ .

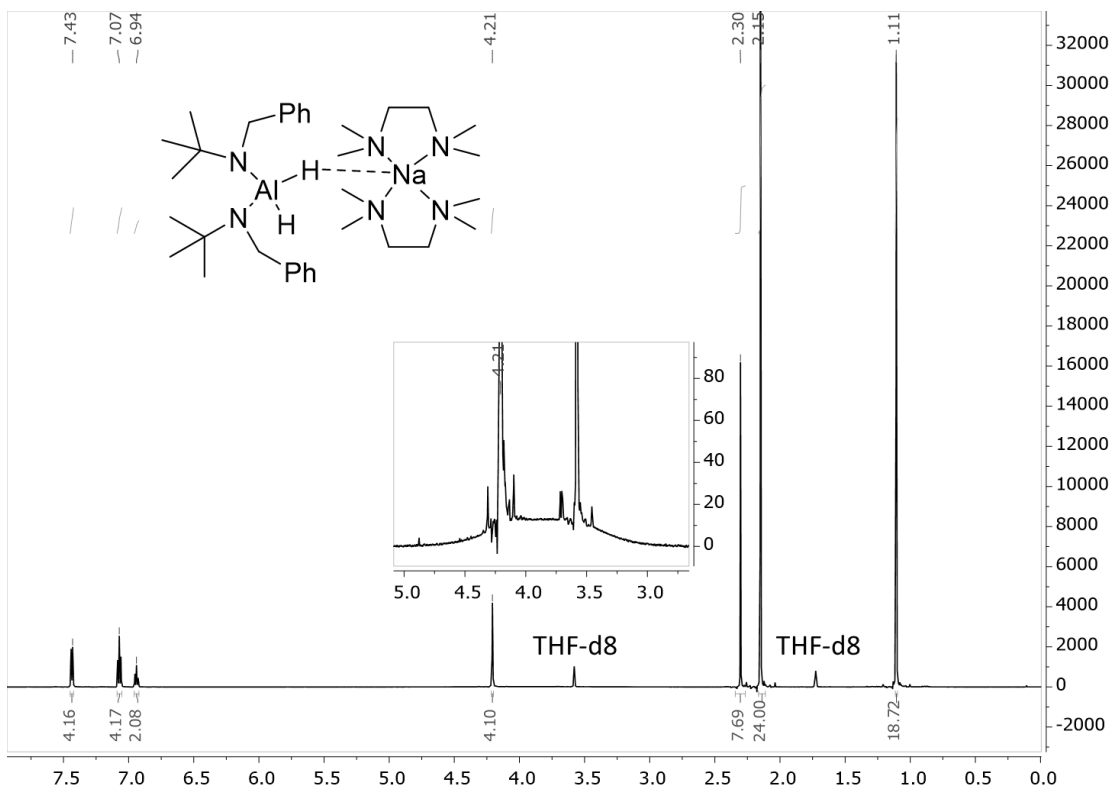


Figure S13:  $^1\text{H}$ -NMR of  $\text{NaAlH}_2[\text{N}(t\text{Bu})\text{CH}_2\text{Ph}]_2 \cdot (\text{TMEDA})_2$  (**2**). NMR in THF- $d_8$ .

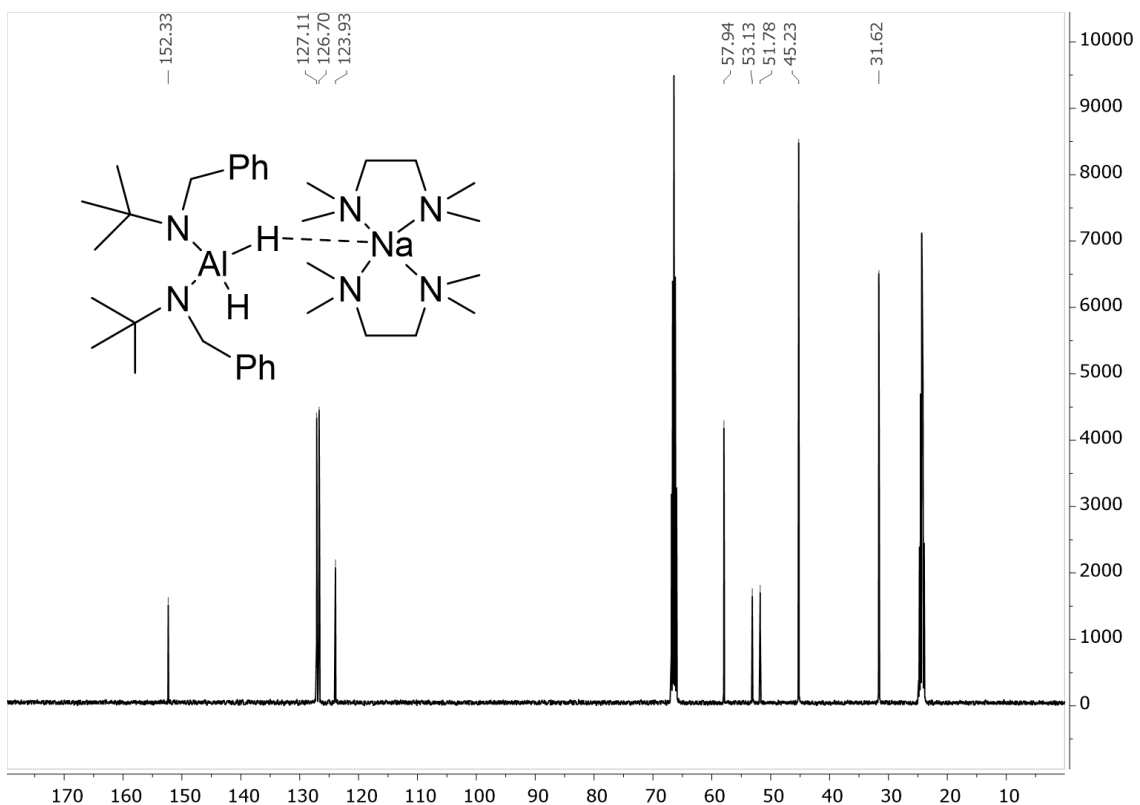


Figure S14:  $^{13}\text{C}$ -NMR of  $\text{NaAlH}_2[\text{N}(t\text{Bu})\text{CH}_2\text{Ph}]_2 \cdot (\text{TMEDA})_2$  (**2**). NMR in THF- $d_8$ .

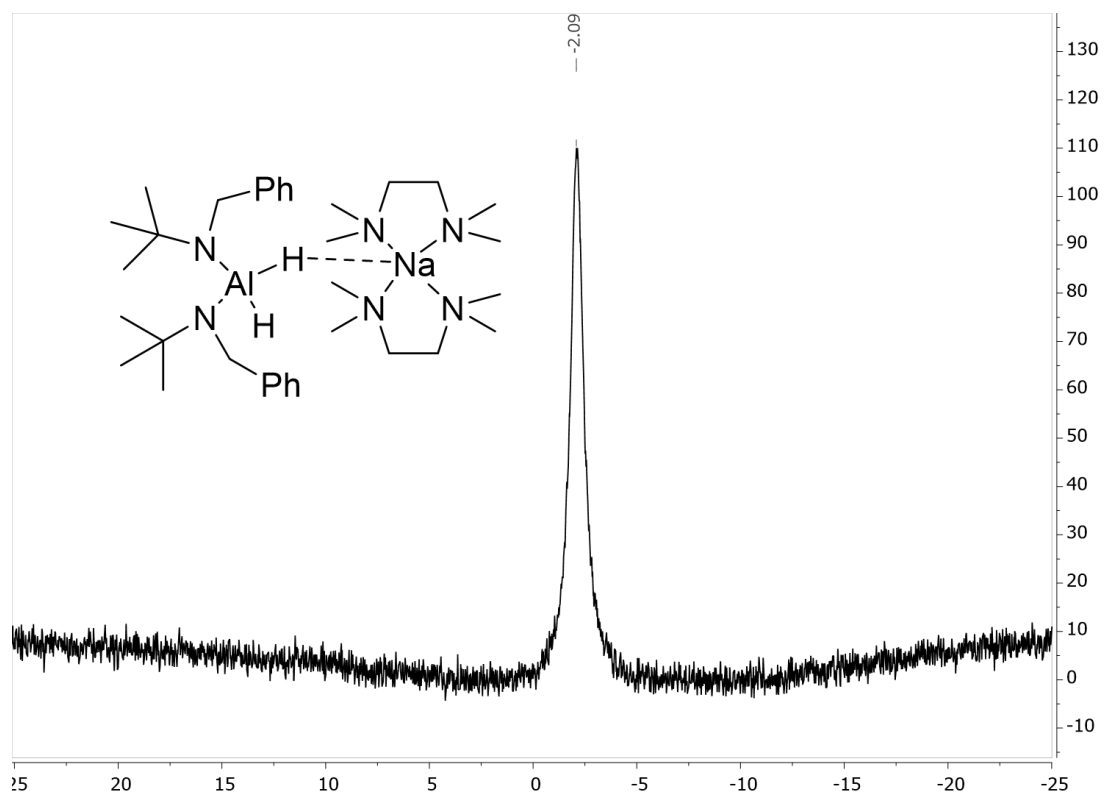


Figure S15:  $^{23}\text{Na}$ -NMR of  $\text{NaAlH}_2[\text{N}(t\text{Bu})\text{CH}_2\text{Ph}]_2 \cdot (\text{TMEDA})_2$  (**2**). NMR in  $\text{THF}-d_8$ .

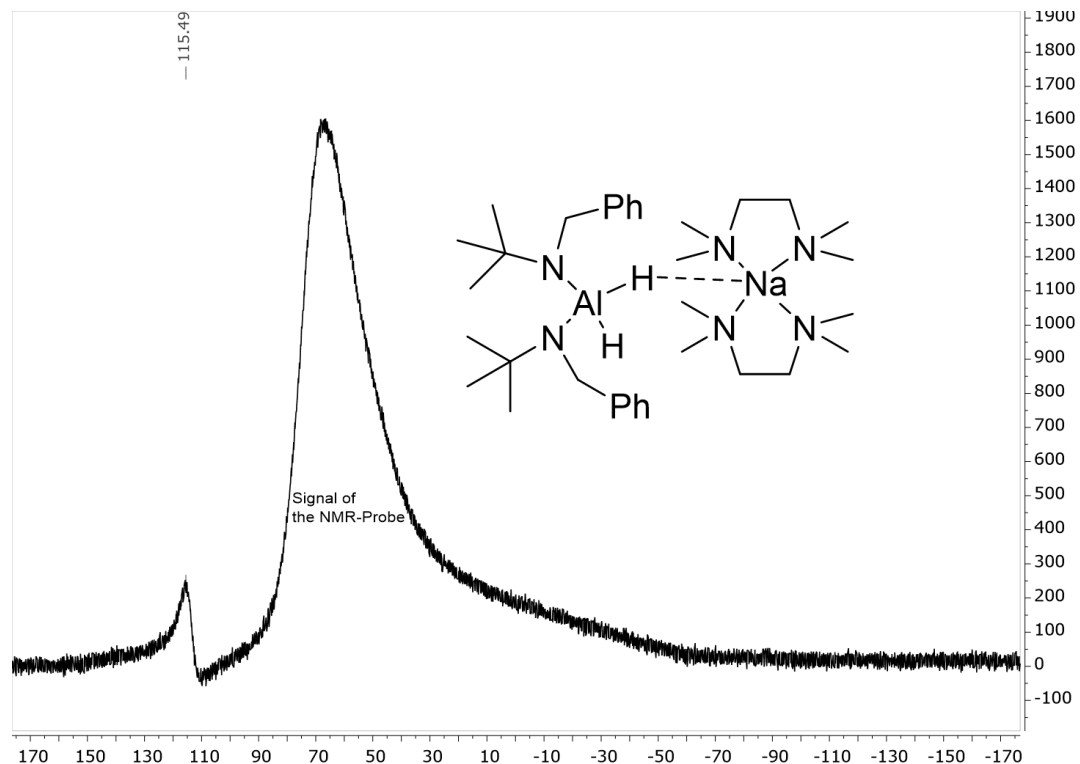


Figure S16:  $^{27}\text{Al}$ -NMR of  $\text{NaAlH}_2[\text{N}(t\text{Bu})\text{CH}_2\text{Ph}]_2 \cdot (\text{TMEDA})_2$  (**2**). NMR in  $\text{THF}-d_8$ .

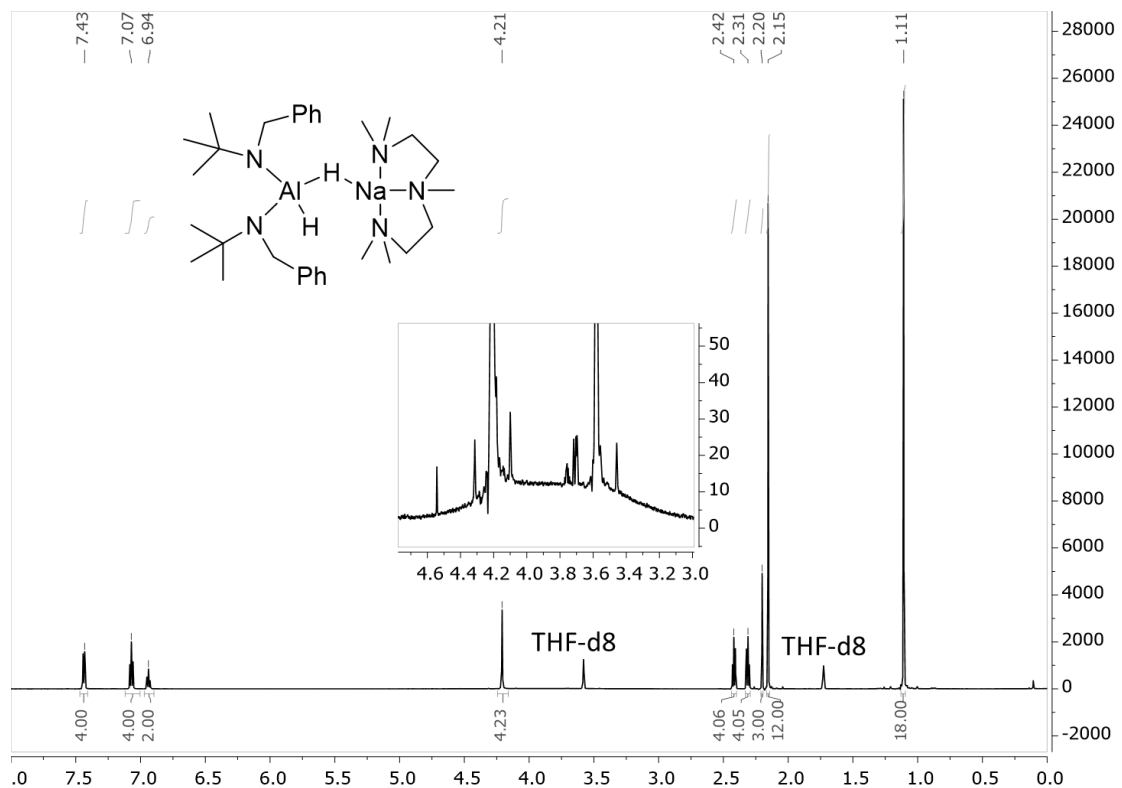


Figure S17: <sup>1</sup>H-NMR of  $\text{NaAlH}_2[\text{N}(t\text{Bu})\text{CH}_2\text{Ph}]_2\cdot\text{PMDTA}$  (**3**). NMR in  $\text{THF}-d_8$ .

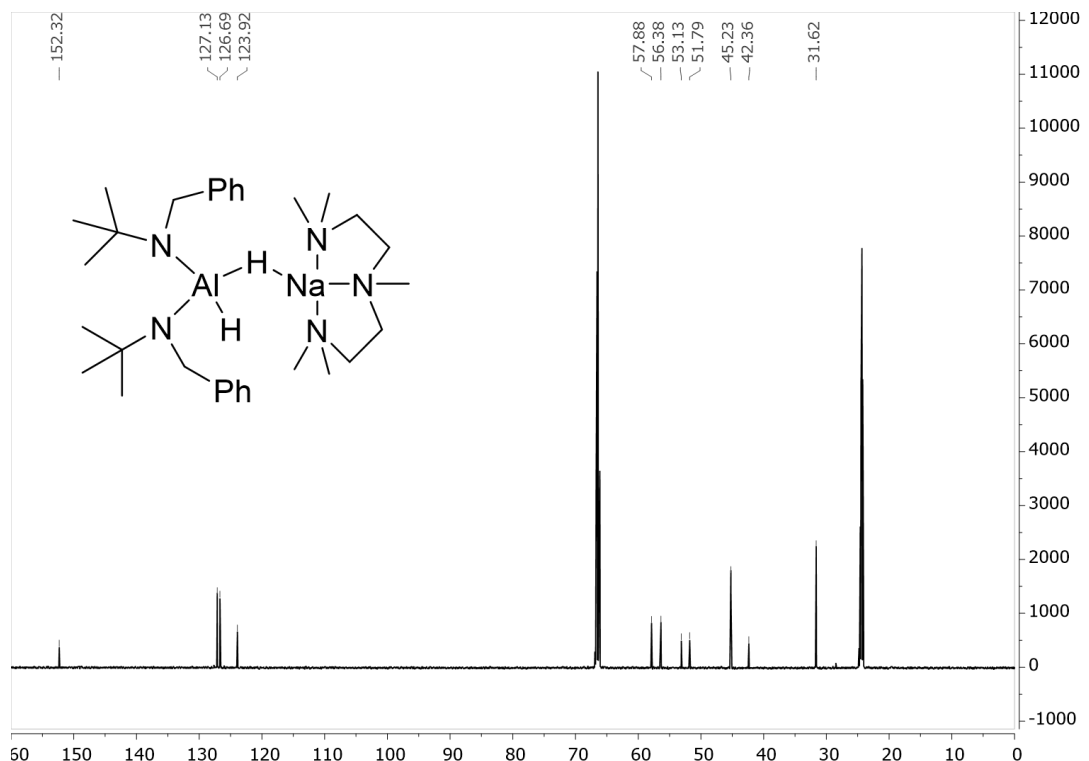


Figure S18: <sup>13</sup>C-NMR of  $\text{NaAlH}_2[\text{N}(t\text{Bu})\text{CH}_2\text{Ph}]_2\cdot\text{PMDTA}$  (**3**). NMR in  $\text{THF}-d_8$ .

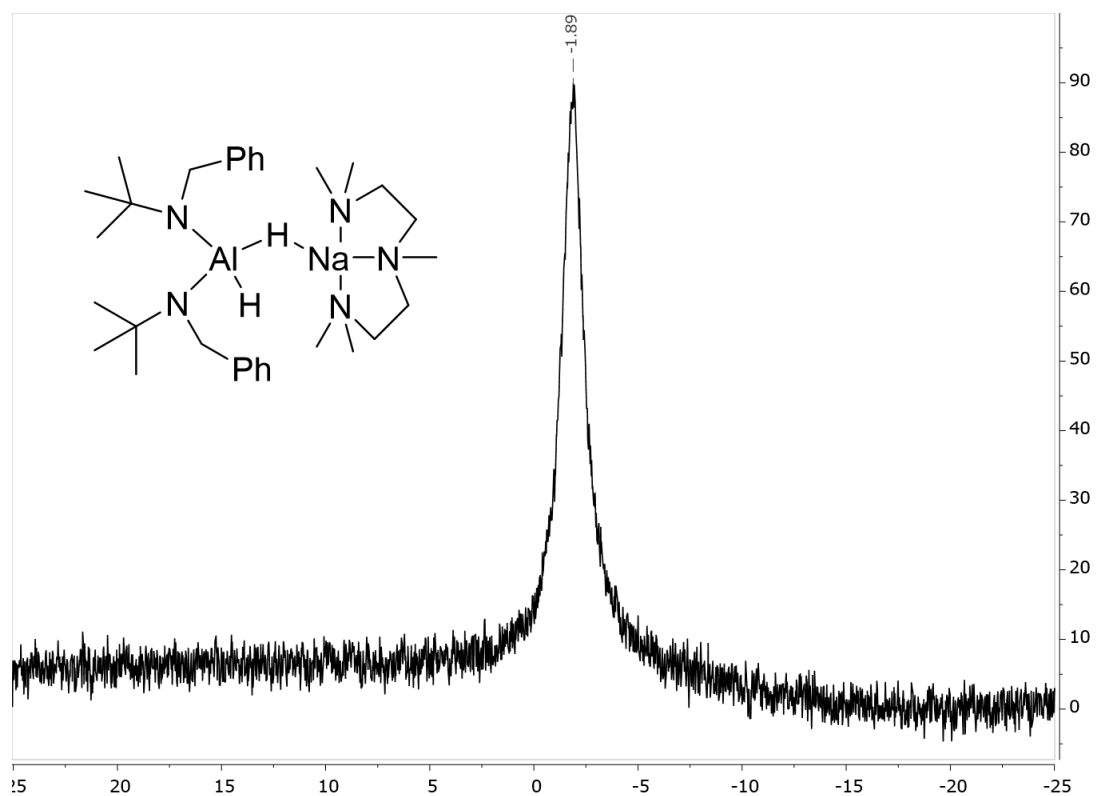


Figure S19:  $^{23}\text{Na}$ -NMR of  $\text{NaAlH}_2[\text{N}(t\text{Bu})\text{CH}_2\text{Ph}]_2 \cdot \text{PMDTA}$  (3). NMR in  $\text{THF}-d_8$ .

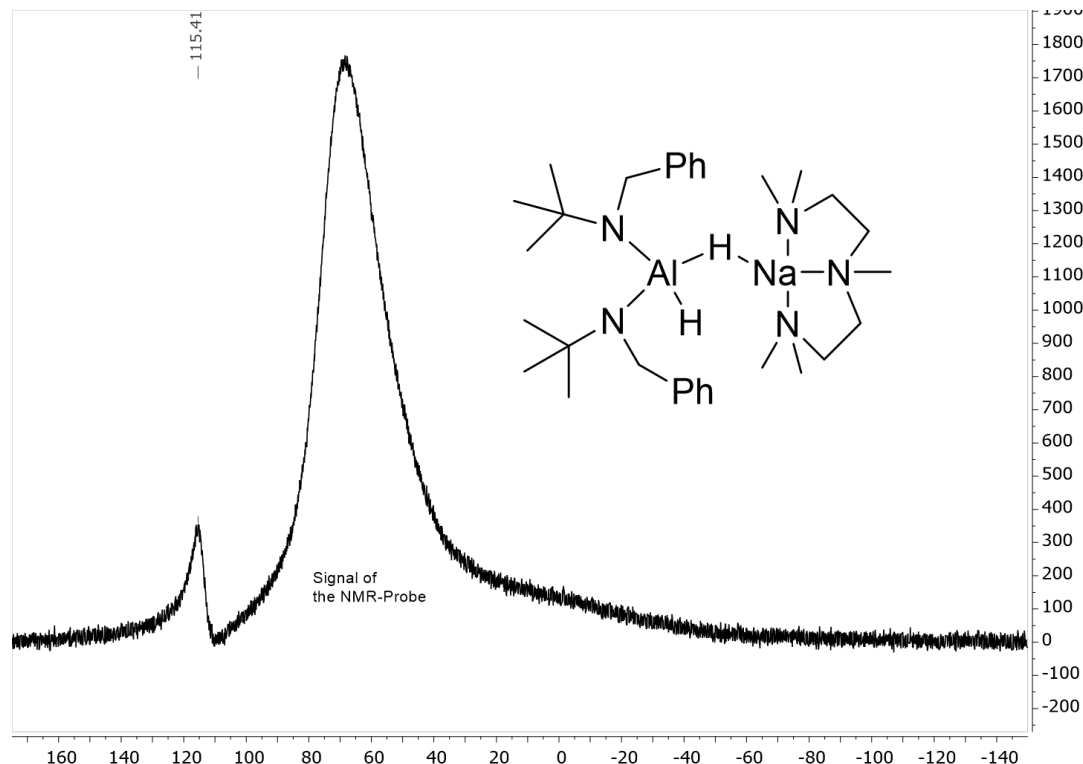


Figure S20:  $^{27}\text{Al}$ -NMR of  $\text{NaAlH}_2[\text{N}(t\text{Bu})\text{CH}_2\text{Ph}]_2 \cdot \text{PMDTA}$  (3). NMR in  $\text{THF}-d_8$ .

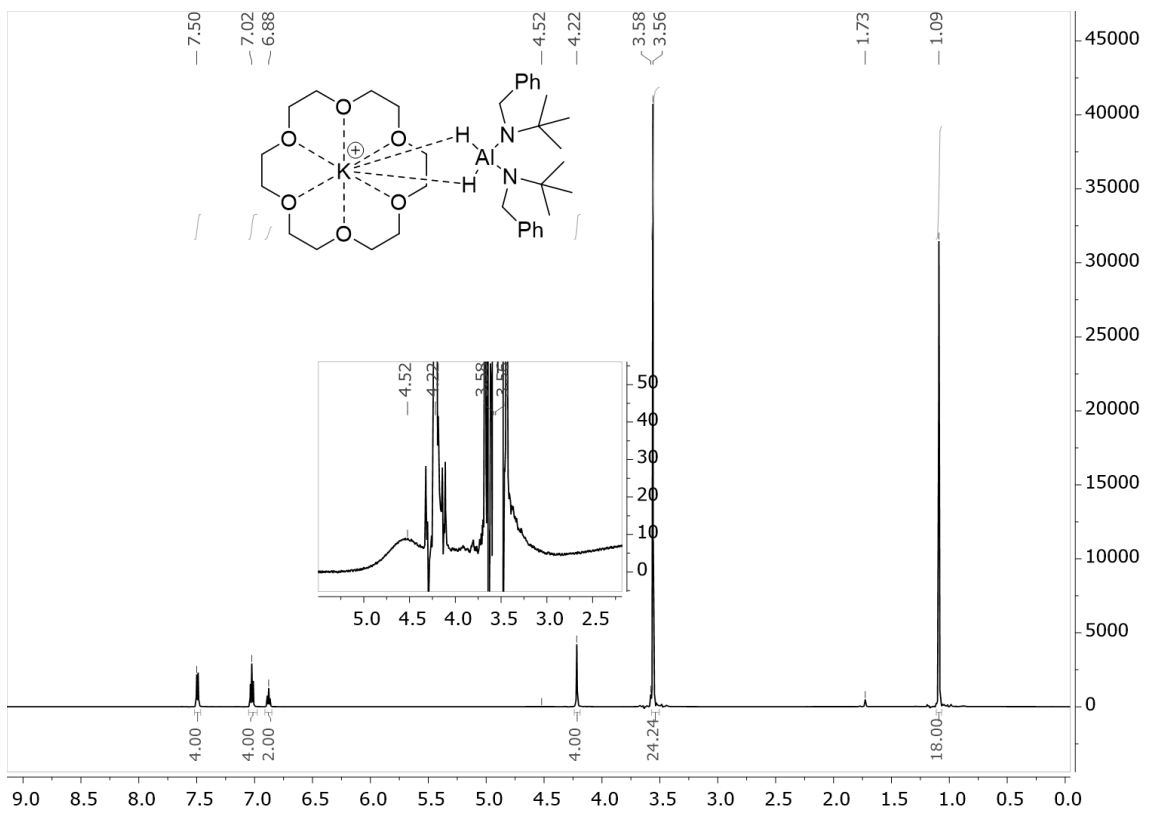


Figure S21:  $^1\text{H}$ -NMR of  $\text{KAlH}_2[\text{N}(t\text{Bu})\text{CH}_2\text{Ph}]_2\cdot18\text{-crown-6}$  (**4**). NMR in  $\text{THF}-d_8$ .

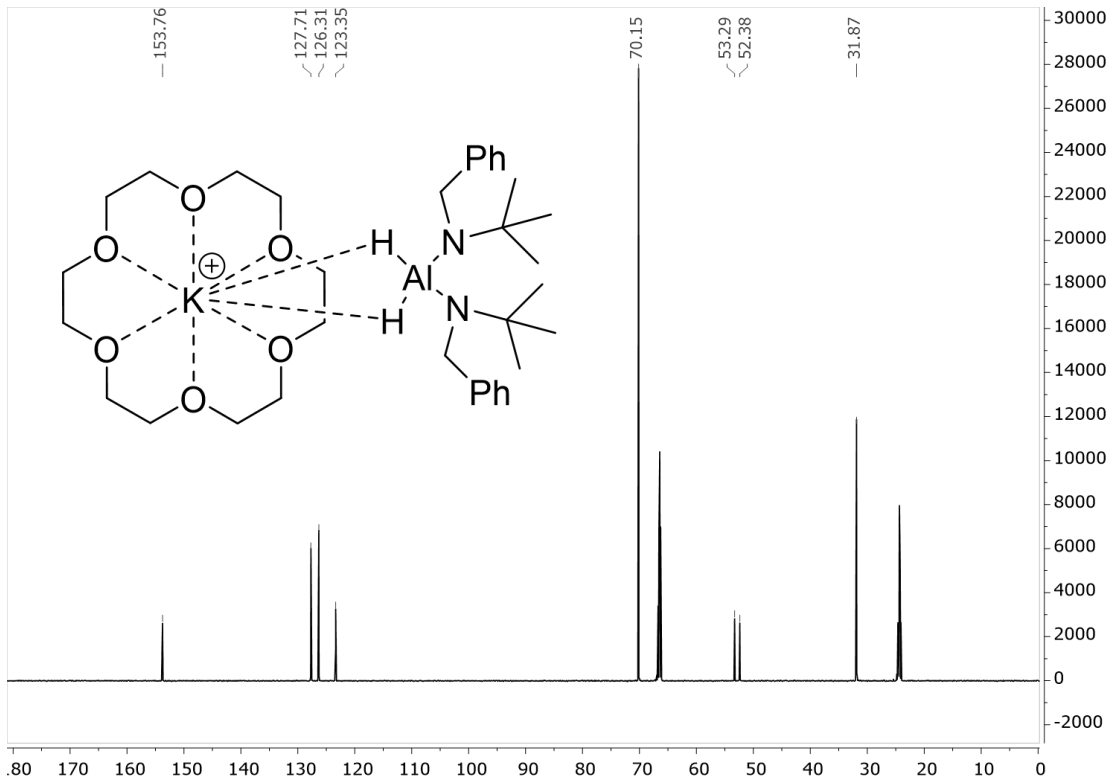


Figure S22:  $^{13}\text{C}$ -NMR of  $\text{KAlH}_2[\text{N}(t\text{Bu})\text{CH}_2\text{Ph}]_2\cdot18\text{-crown-6}$  (**4**). NMR in  $\text{THF}-d_8$ .

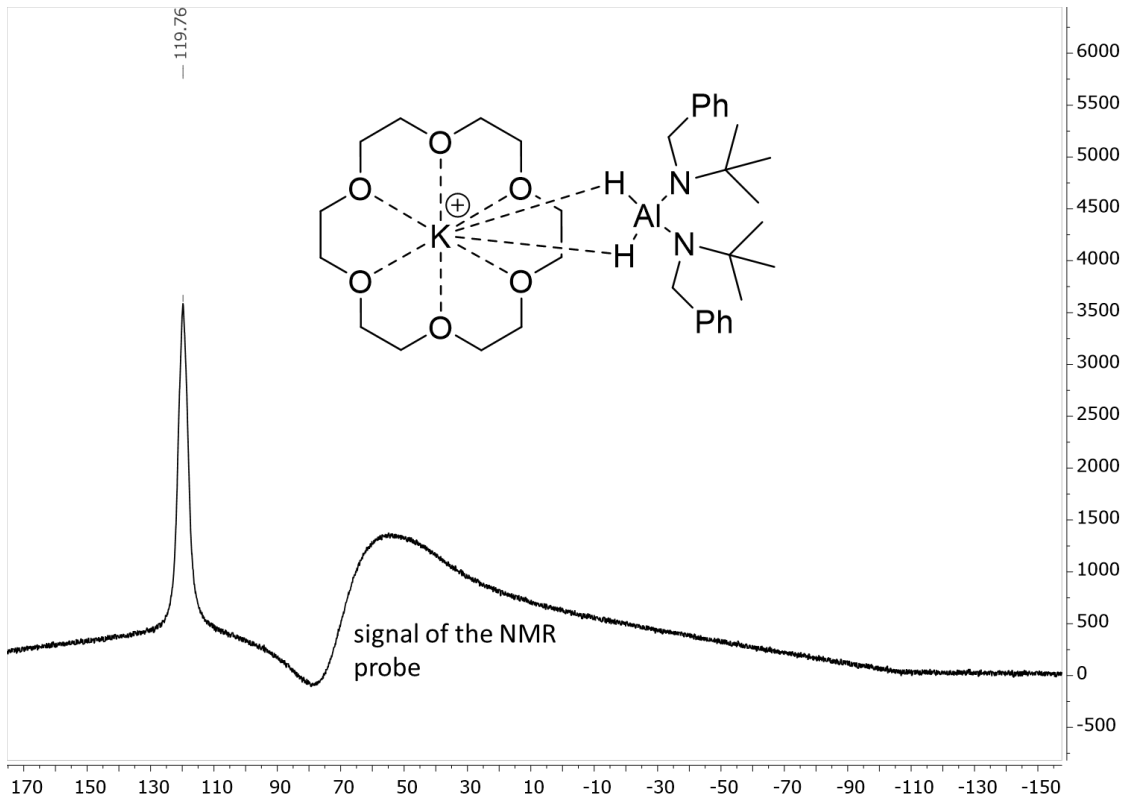


Figure S23:  $^{27}\text{Al}$ -NMR of  $\text{KAIH}_2[\text{N}(t\text{Bu})\text{CH}_2\text{Ph}]_2\cdot18\text{-crown-6}$  (**4**). NMR in  $\text{THF}-d_8$ .

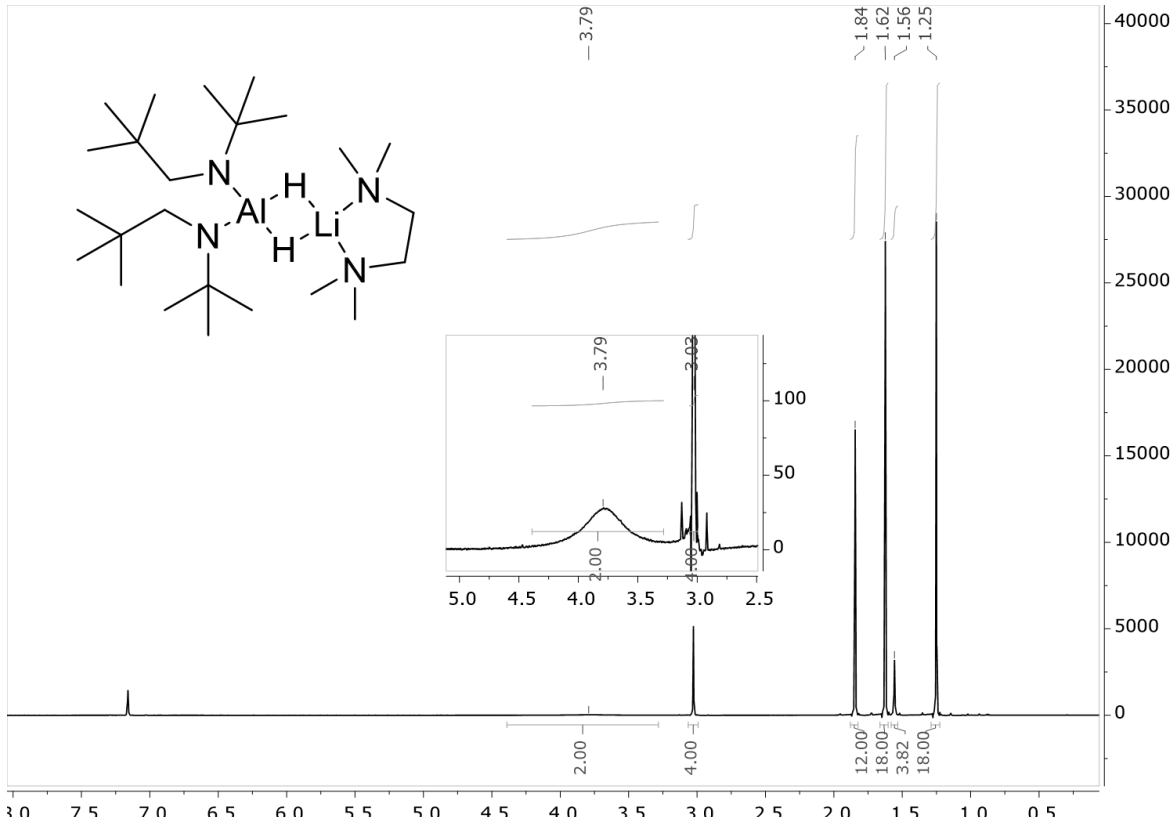


Fig. S24:  $^1\text{H}$ -NMR of  $\text{LiAlH}_2[\text{N}(t\text{Bu})\text{CH}_2t\text{Bu}]_2\cdot(\text{TMEDA})$  (**5**). NMR in  $\text{C}_6\text{D}_6$ .

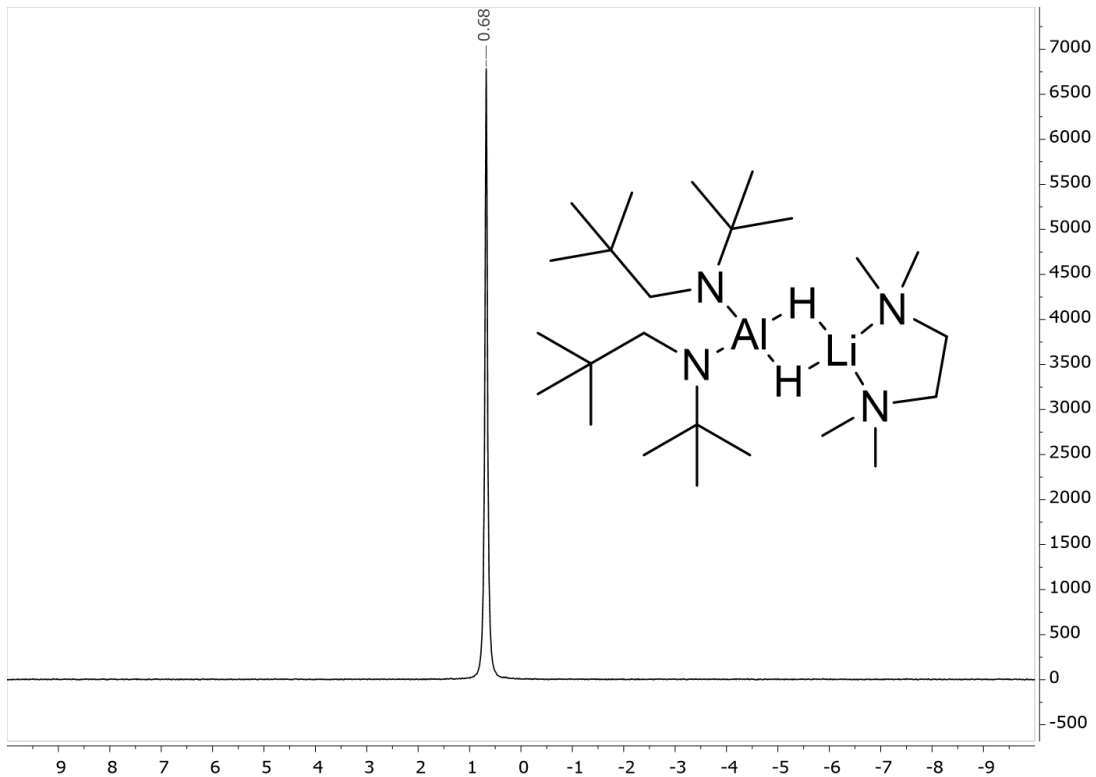


Fig. S25:  ${}^7\text{Li}$ -NMR of  $\text{LiAlH}_2[\text{N}(t\text{Bu})\text{CH}_2t\text{Bu}]_2 \cdot (\text{TMEDA})$  (5). NMR in  $\text{C}_6\text{D}_6$ .

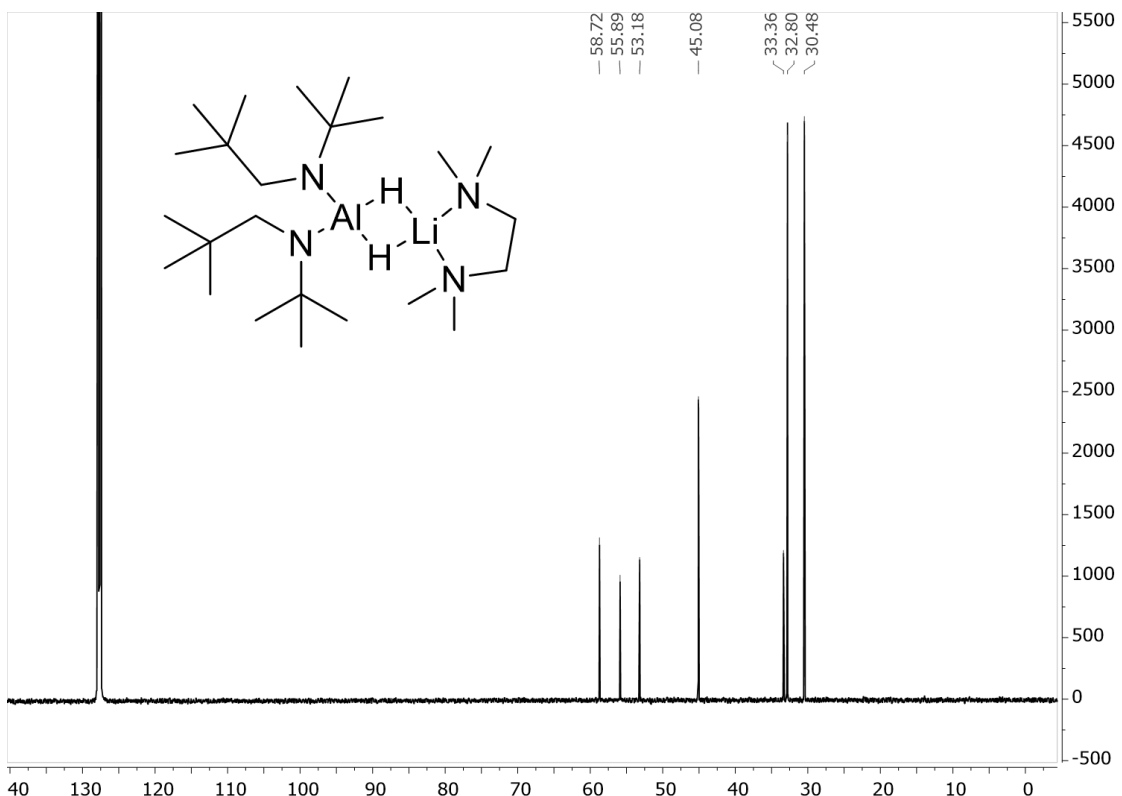


Fig. S26:  ${}^{13}\text{C}$ -NMR of  $\text{LiAlH}_2[\text{N}(t\text{Bu})\text{CH}_2t\text{Bu}]_2 \cdot (\text{TMEDA})$  (5). NMR in  $\text{C}_6\text{D}_6$ .

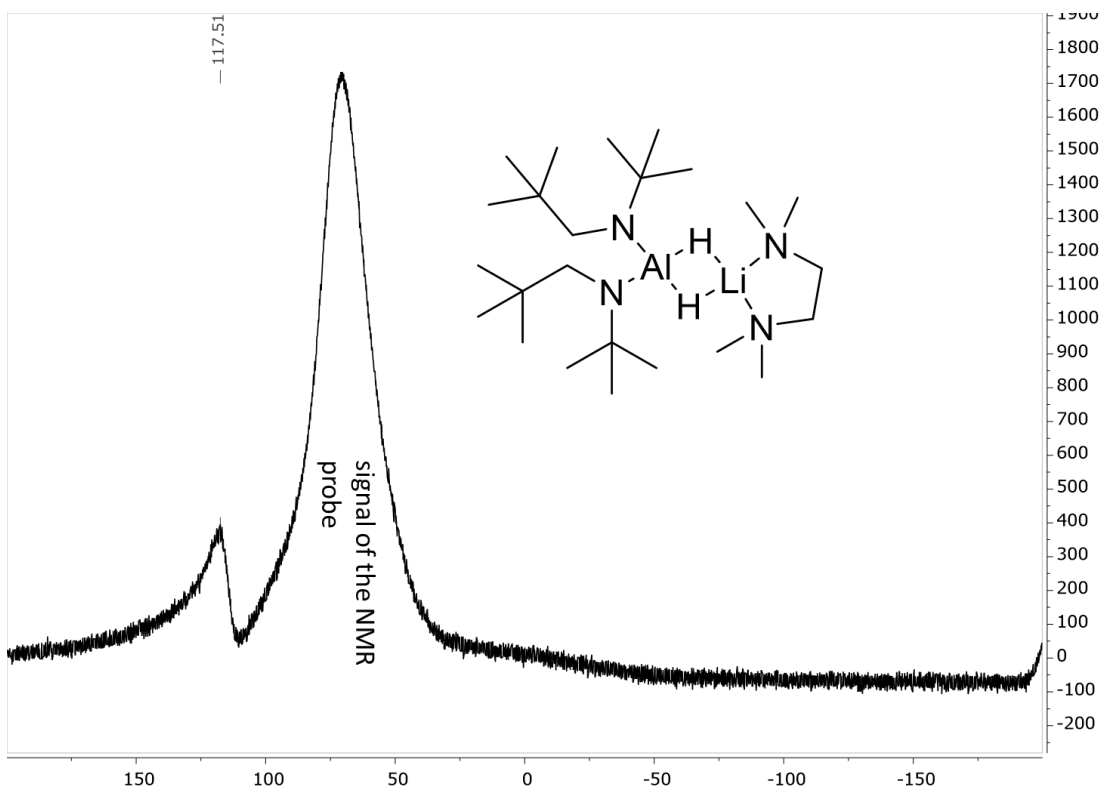


Fig. S27:  $^{27}\text{Al}$ -NMR of  $\text{LiAlH}_2[\text{N}(i\text{-Bu})\text{CH}_2\text{t-Bu}]_2\cdot(\text{TMEDA})$  (**5**). NMR in  $\text{C}_6\text{D}_6$ .

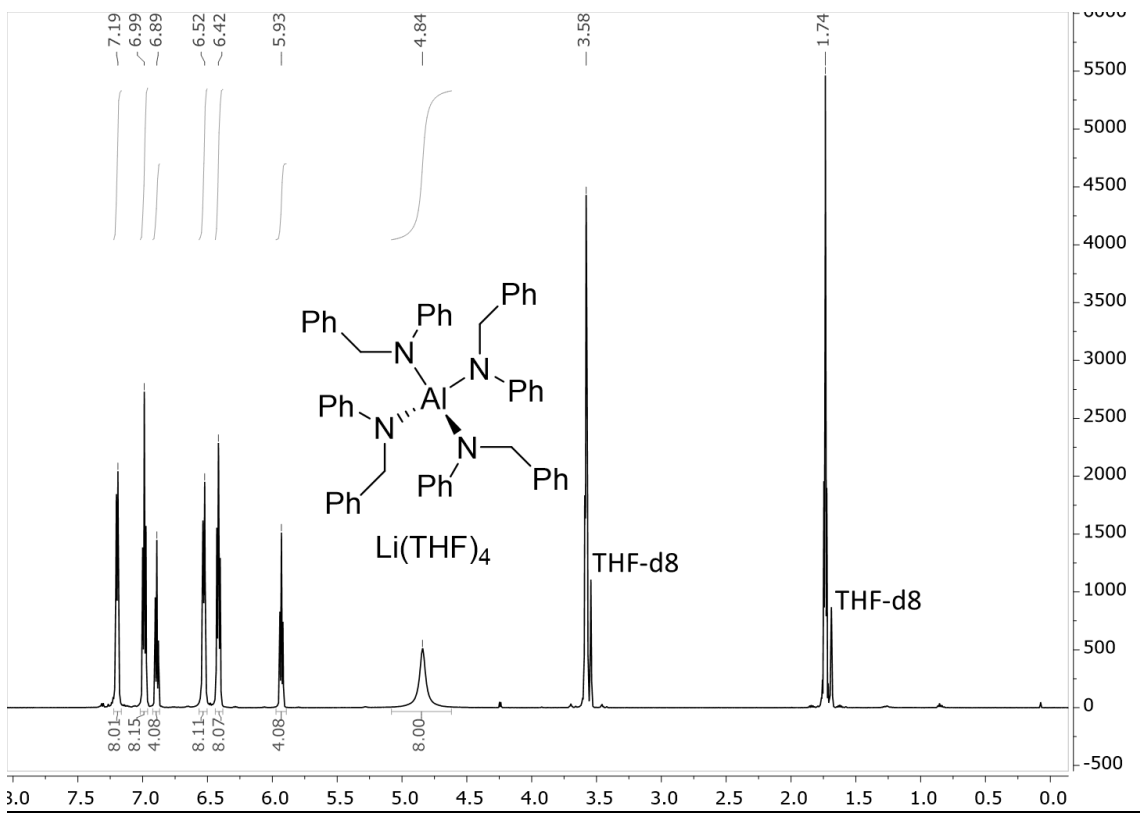


Figure S28:  $^1\text{H}$ -NMR of  $\text{LiAl}[\text{N}(\text{Ph})\text{CH}_2\text{Ph}]_4\cdot(\text{THF})_4$  (**6**). NMR in  $\text{THF}-d_8$ .

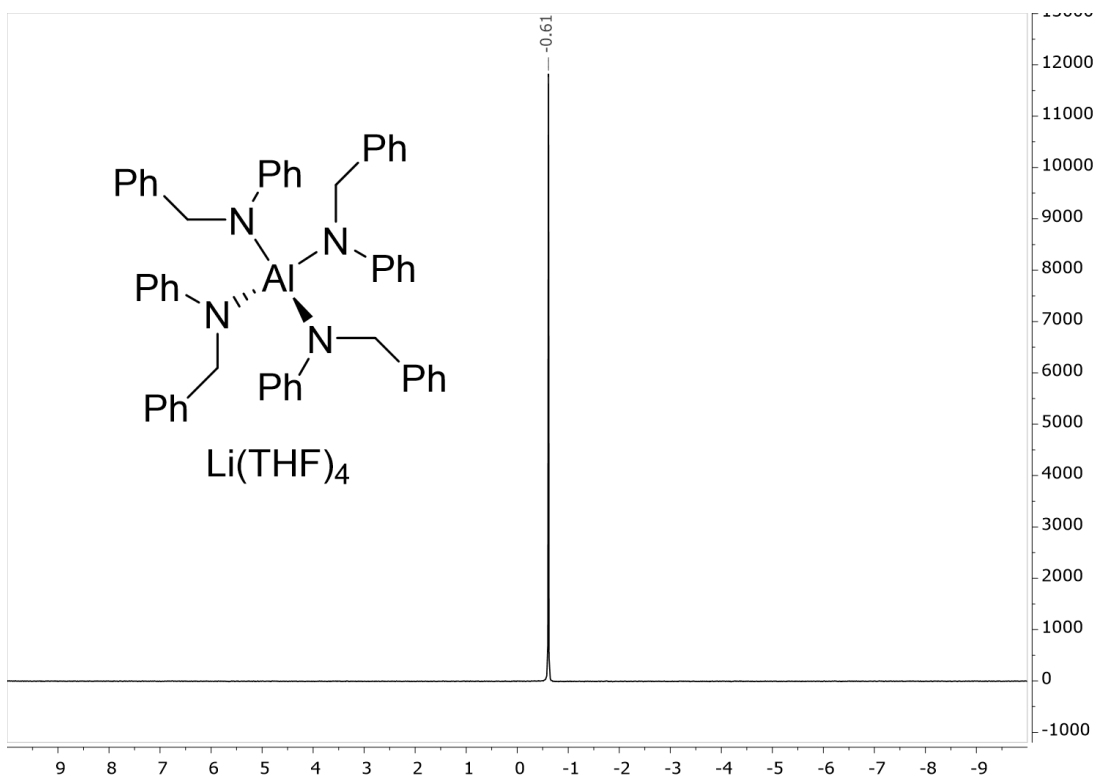


Figure S29:  $^7\text{Li}$ -NMR of  $\text{LiAl}[\text{N}(\text{Ph})\text{CH}_2\text{Ph}]_4 \cdot (\text{THF})_4$  (6). NMR in  $\text{THF}-d_8$ .

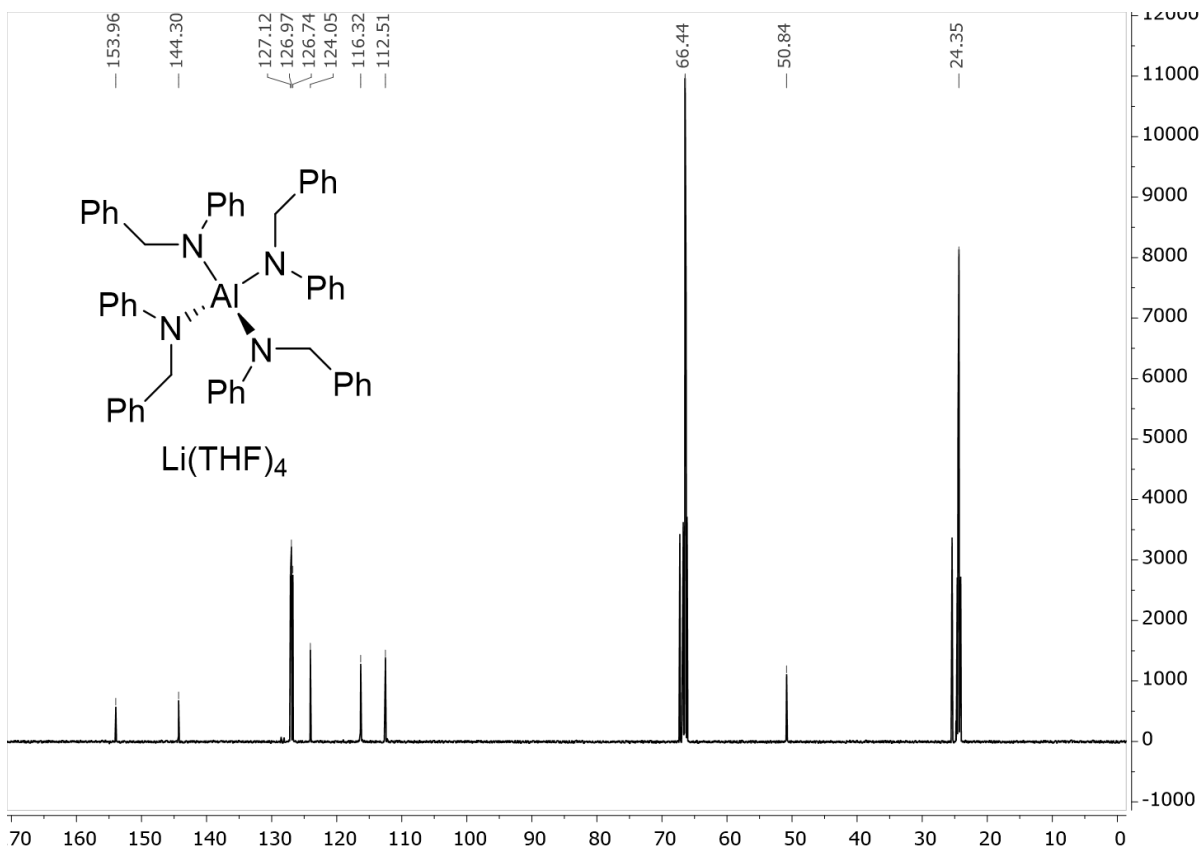


Figure S30:  $^{13}\text{C}$ -NMR of  $\text{LiAl}[\text{N}(\text{Ph})\text{CH}_2\text{Ph}]_4 \cdot (\text{THF})_4$  (6). NMR in  $\text{THF}-d_8$ .

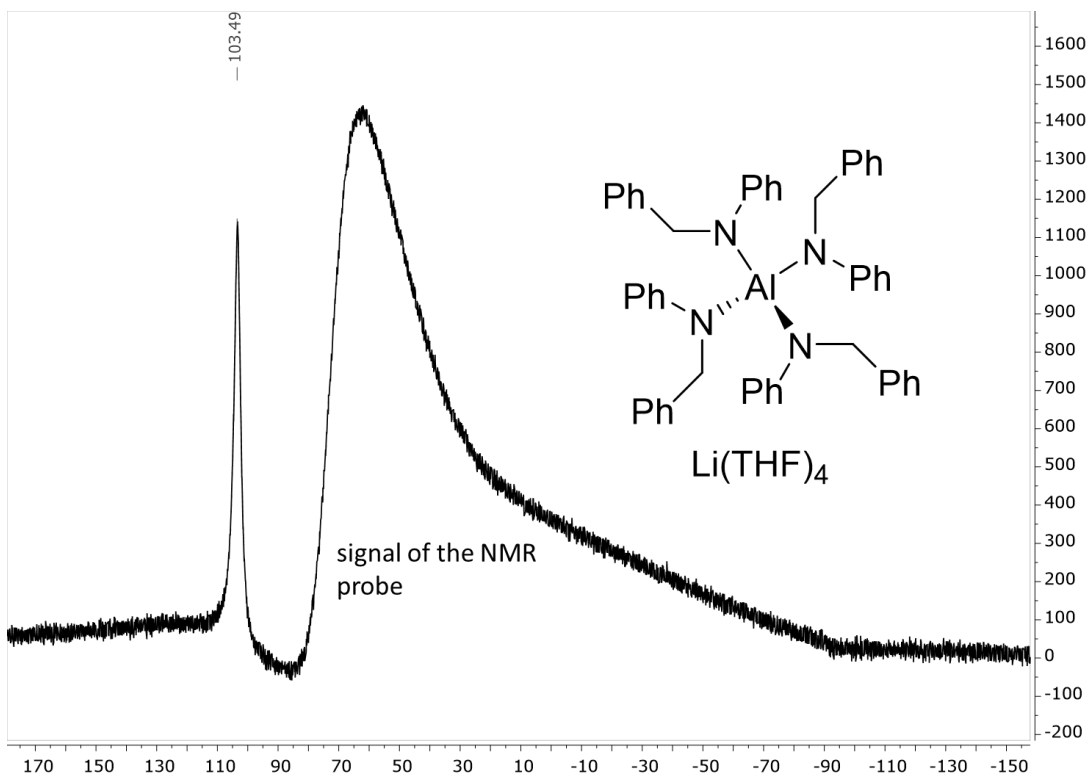


Figure S31:  $^{27}\text{Al}$ -NMR of  $\text{LiAl}[\text{N}(\text{Ph})\text{CH}_2\text{Ph}]_4 \cdot (\text{THF})_4$  (**6**). NMR in  $\text{THF}-d_8$ .

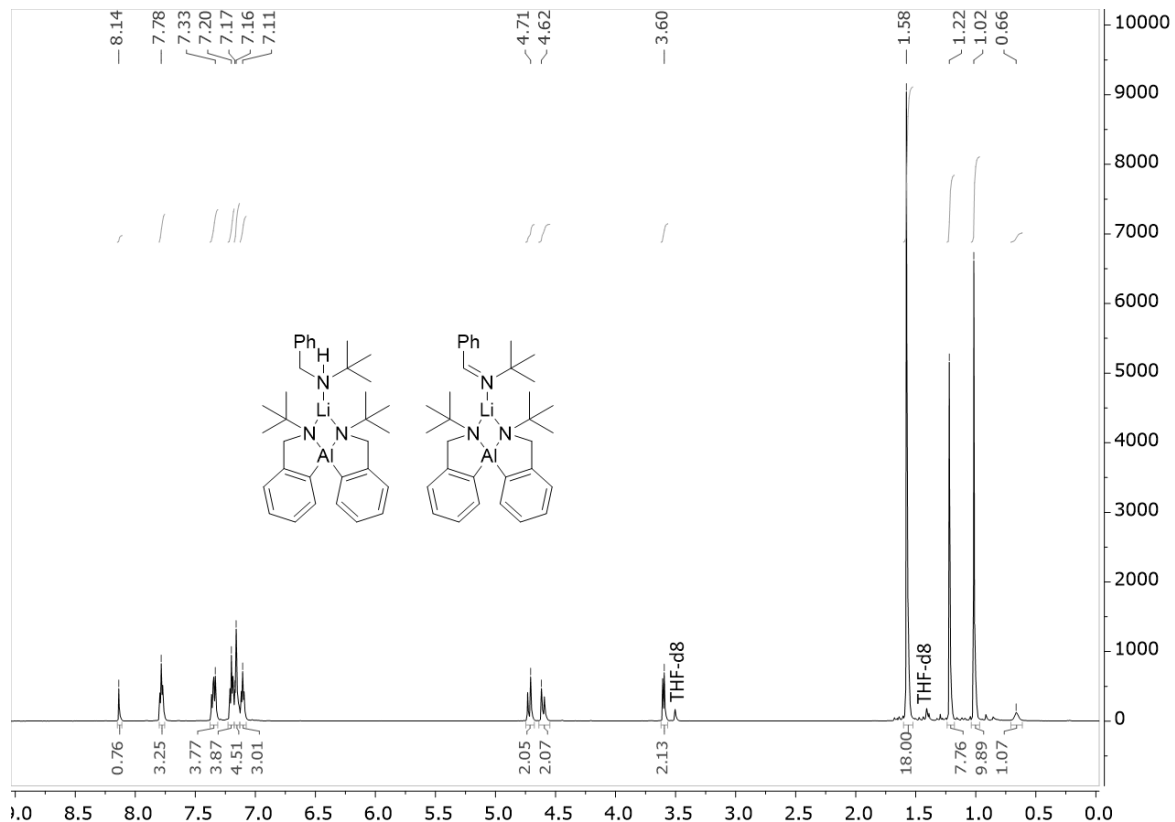


Figure S32:  $^1\text{H}$ -NMR of complex **7**. NMR in  $\text{C}_6\text{D}_6/\text{THF}-d_8$  5/1.

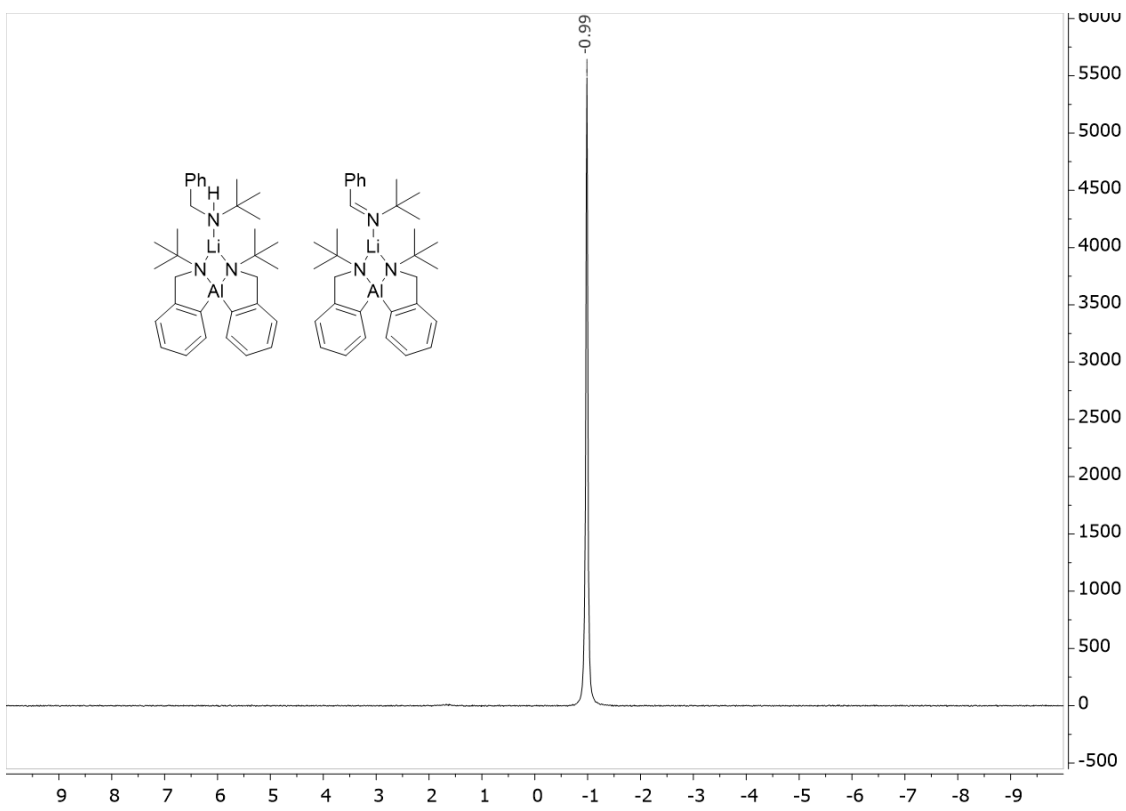


Figure S33: <sup>7</sup>Li-NMR of **7**. NMR in C<sub>6</sub>D<sub>6</sub>/THF-d<sub>8</sub> 5/1.

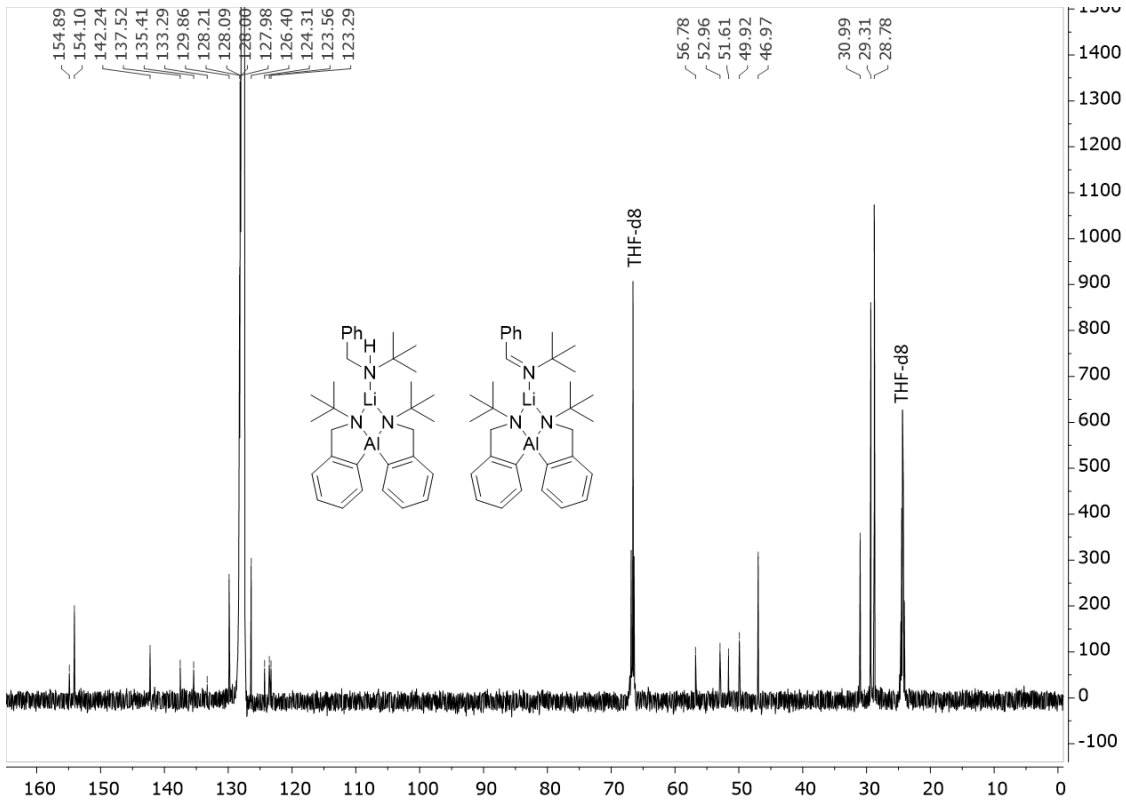


Figure S34: <sup>13</sup>C-NMR of **7**. NMR in C<sub>6</sub>D<sub>6</sub>/THF-d<sub>8</sub> 5/1.

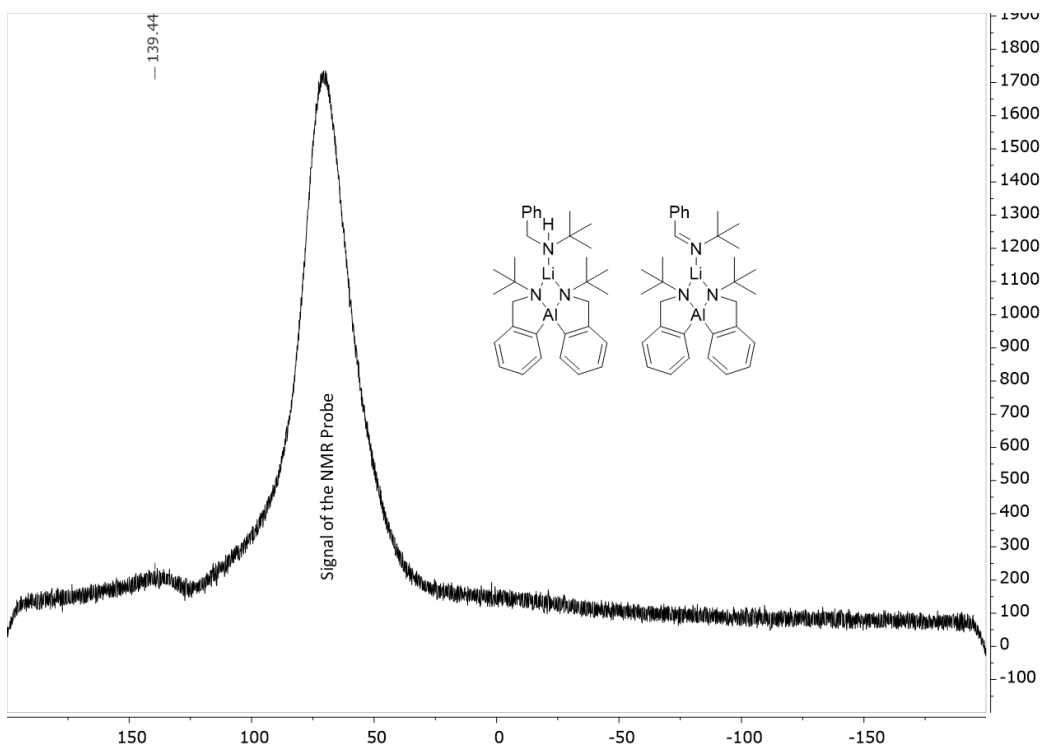


Figure S35:  $^{27}\text{Al}$ -NMR of **7**. NMR in  $\text{C}_6\text{D}_6/\text{THF}-d_8$  5/1.

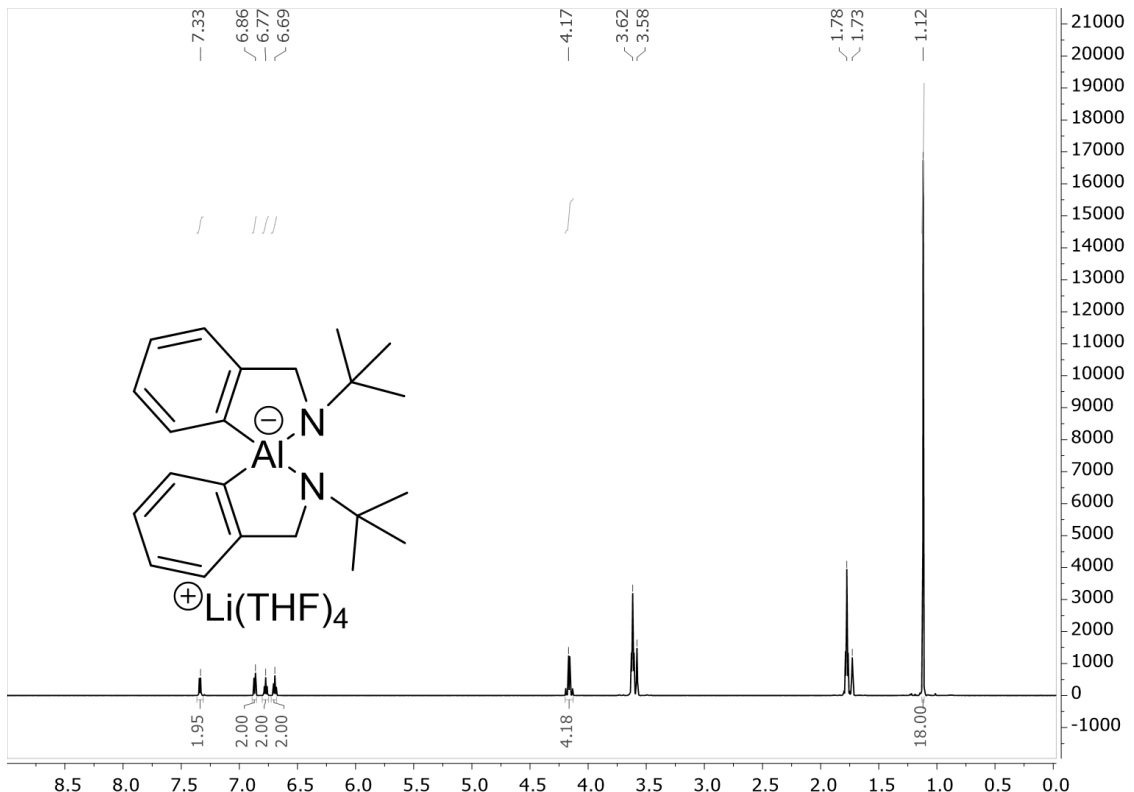


Figure S36:  $^1\text{H}$ -NMR of complex **8**. NMR in  $\text{THF}-d_8$ .

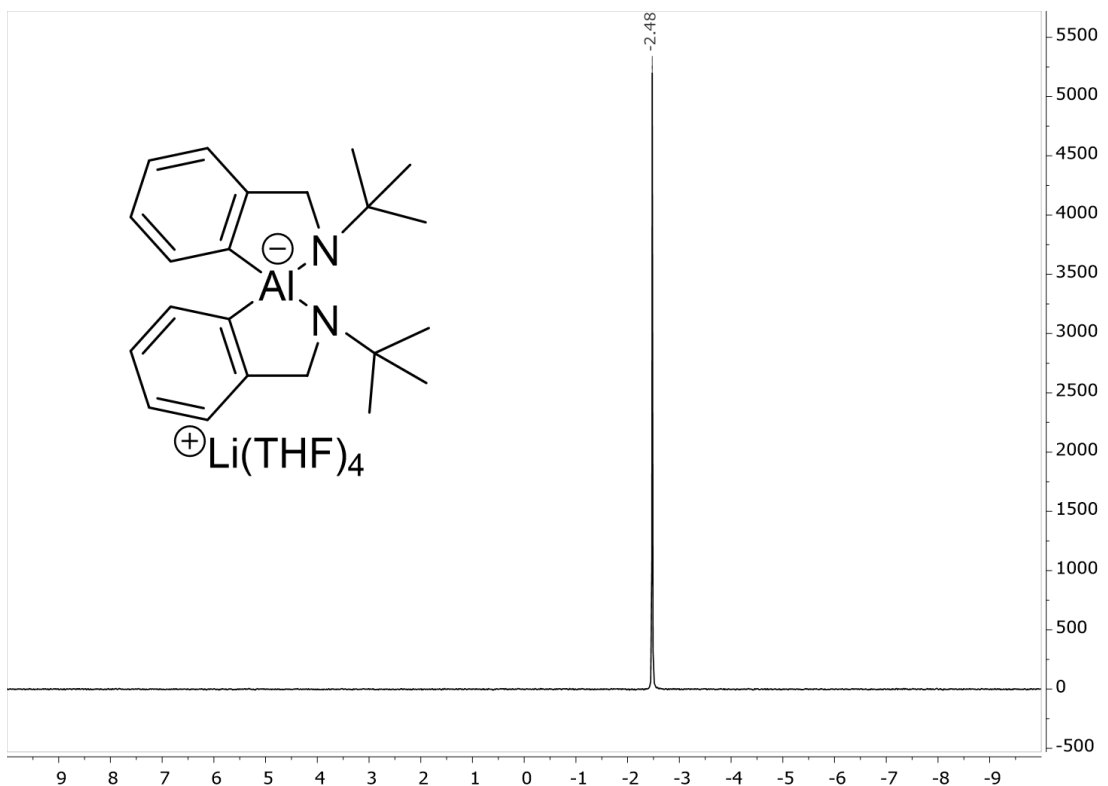


Figure S37: <sup>7</sup>Li-NMR of complex 8. NMR in THF-*d*<sub>8</sub>.

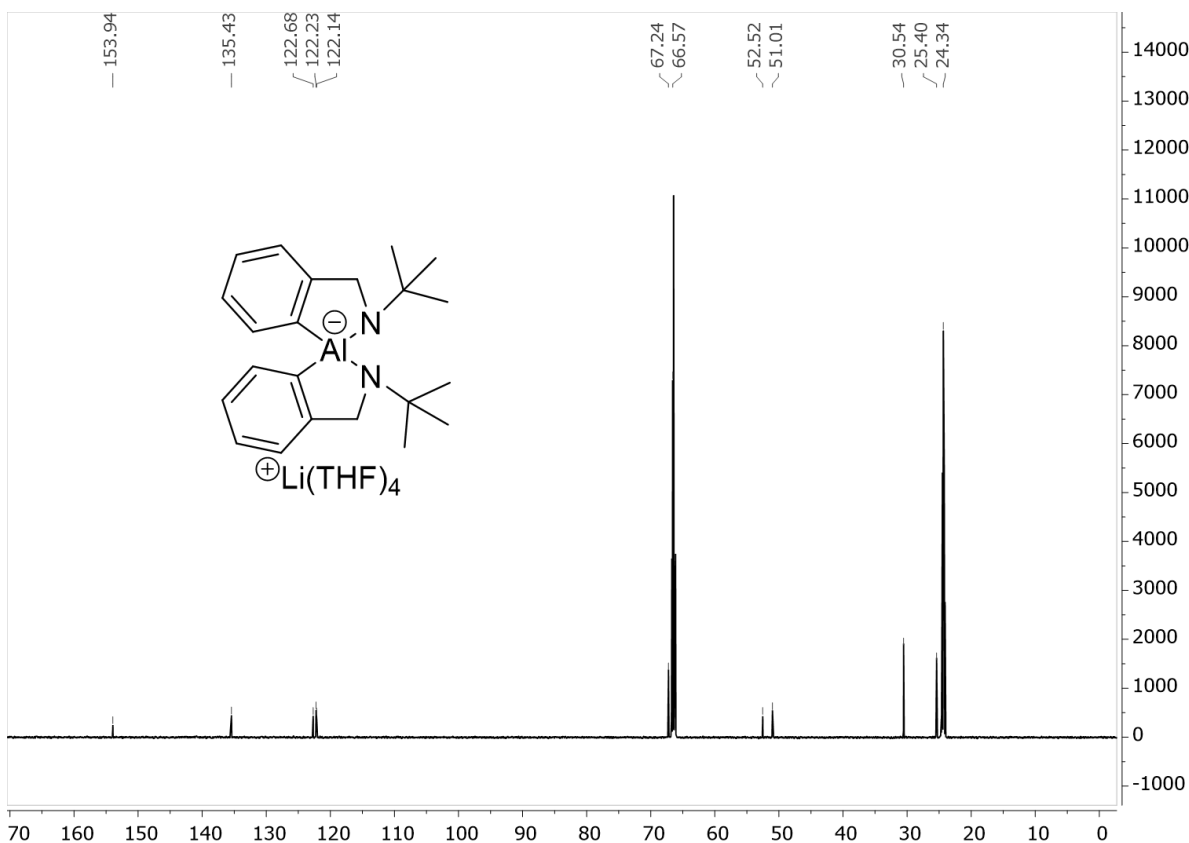


Figure S38: <sup>13</sup>C-NMR of complex 8. NMR in THF-*d*<sub>8</sub>.

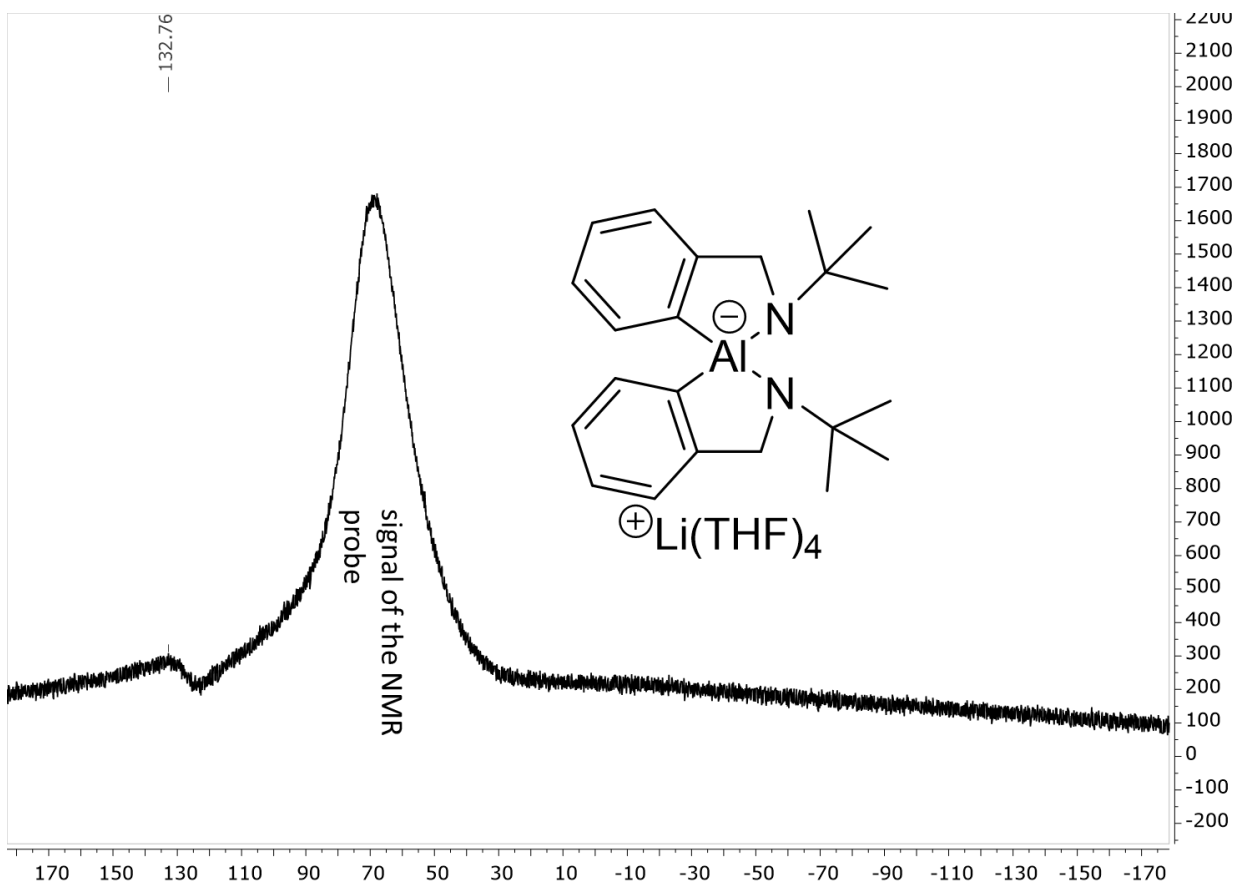


Figure S39:  $^{27}\text{Al}$ -NMR of complex **8**. NMR in  $\text{THF}-d_8$ .

## Crystal Structures

### Structure determination of $\text{LiAlH}[\text{N}(t\text{Bu})\text{CH}_2\text{Ph}]_3 \cdot (\text{THF})_4$ (1)

A colorless crystal of  $\text{LiAlH}[\text{N}(t\text{Bu})\text{CH}_2\text{Ph}]_3 \cdot (\text{THF})_4$  was embedded in inert perfluoropolyalkylether (viscosity 1800 cSt; ABCR GmbH) and mounted using a Hampton Research CryoLoop. The crystal was then flash cooled to 100.0(1) K in a nitrogen gas stream and kept at this temperature during the experiment. The crystal structure was measured on a SuperNova diffractometer with Atlas S2 detector using a  $\text{CuK}\alpha$  microfocus source. The measured data was processed with the CrysAlisPro (v40.67a) software package.<sup>[59]</sup> Using Olex2,<sup>[55]</sup> the structure was solved with the ShelXT<sup>[56]</sup> structure solution program using Intrinsic Phasing and refined with the ShelXL<sup>[57]</sup> refinement package using Least Squares Minimization. Most hydrogen atoms were placed in ideal positions and refined as riding atoms with relative isotropic displacement parameters. The metal bound hydride was observed from difference Fourier maps and refined.

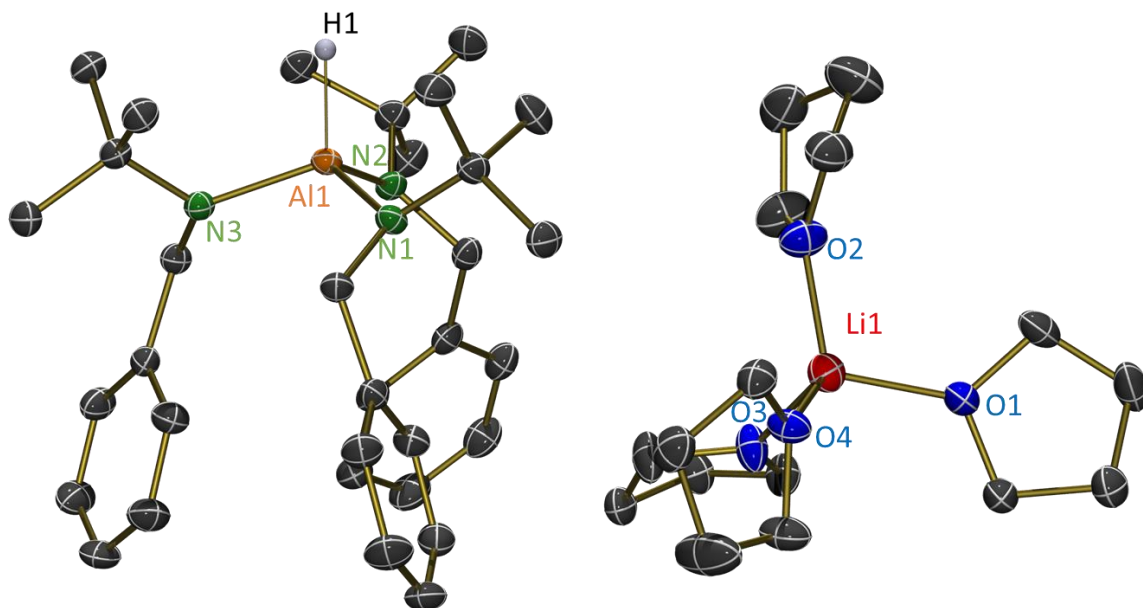


Figure S40: ORTEP-plot (50% probability) of  $\text{LiAlH}[\text{N}(t\text{Bu})\text{CH}_2\text{Ph}]_3 \cdot (\text{THF})_4$  (1). H atoms except for the one bound to Al are omitted for clarity.

### Structure determination of $\text{NaAlH}_2[\text{N}(t\text{Bu})\text{CH}_2\text{Ph}]_2 \cdot (\text{TMEDA})_2$ (2)

A colorless crystal of compound **1** was embedded in inert perfluoropolyalkylether (viscosity 1800 cSt; ABCR GmbH) and mounted using a Hampton Research CryoLoop. The crystal was then flash cooled to 100.00(11) K in a nitrogen gas stream and kept at this temperature during the experiment. The crystal structure was measured on a SuperNova diffractometer with Atlas S2 detector using a  $\text{CuK}\alpha$  microfocus source. The measured data was processed with the CrysAlisPro (v40.53) software package.<sup>[54]</sup> Using Olex2<sup>[55]</sup>, the structure was solved with the ShelXT<sup>[56]</sup> structure solution program using Intrinsic Phasing and refined with the ShelXL<sup>[57]</sup> refinement package using Least Squares minimization. All non-hydrogen atoms were refined anisotropically. Most hydrogen atoms were placed in ideal positions and refined as riding atoms with relative isotropic displacement parameters. The positions of the aluminum bound hydrides were observed from difference Fourier maps and refined. Disorder of one TMEDA ligand was observed and was modeled with the help of a rigid bond restraint (RIGU)<sup>[58]</sup>. The relative occupancies of the two alternative orientations were refined to 0.39/0.61.

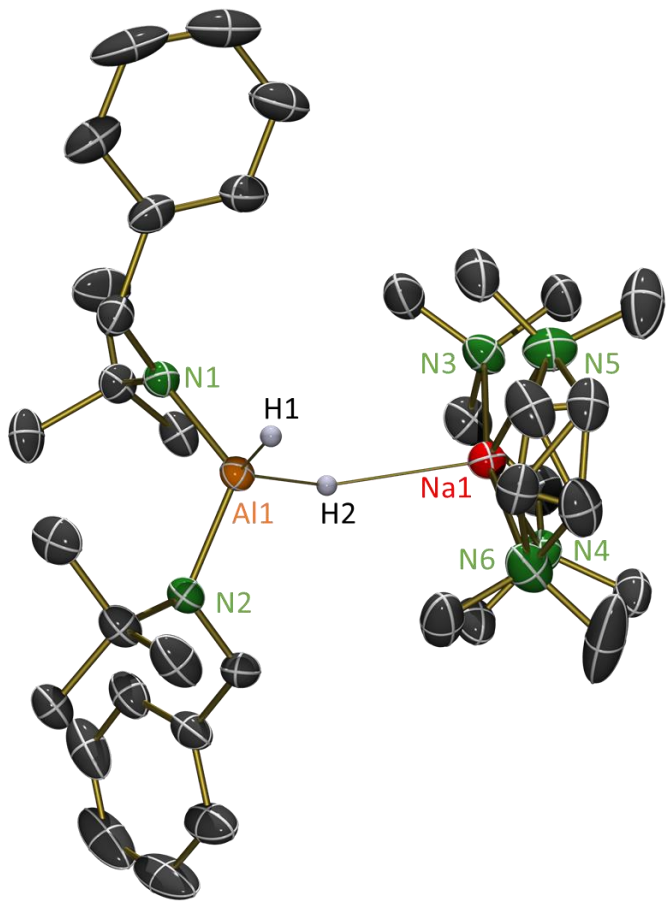


Figure S41: ORTEP-plot (50% probability) of  $\text{NaAlH}_2[\text{N}(t\text{Bu})\text{CH}_2\text{Ph}]_2 \cdot (\text{TMEDA})_2$  (**2**). H atoms except for those bound to Al are omitted for clarity.

### Structure determination of $\text{NaAlH}_2[\text{N}(t\text{Bu})\text{CH}_2\text{Ph}]_2 \cdot \text{PMDTA}$ (3)

A colorless crystal of  $[(\text{pmdta})\text{Na}(\text{H})_2\text{Al}(t\text{BuNCH}_2\text{C}_6\text{H}_5)_2]$  was embedded in inert perfluoropolyalkylether (viscosity 1800 cSt; ABCR GmbH) and mounted using a Hampton Research CryoLoop. The crystal was then

flash cooled to 100.0(2) K in a nitrogen gas stream and kept at this temperature during the experiment. The crystal structure was measured on a SuperNova diffractometer with Atlas S2 detector using a CuK $\alpha$  microfocus source. The measured data was processed with the CrysAlisPro (v40.53) software package.<sup>[S4]</sup> Using Olex2,<sup>[S5]</sup> the structure was solved with the ShelXT<sup>[S6]</sup> structure solution program using Intrinsic Phasing and refined with the ShelXL<sup>[S7]</sup> refinement package using Least Squares Minimization. All non-hydrogen atoms were refined anisotropically. Most hydrogen atoms were placed in ideal positions and refined as riding atoms with relative isotropic displacement parameters. The metal bound hydrides were observed from difference Fourier maps and refined.

Disorder of one benzyl group and of the pmdta ligand was observed. The disorder was modeled with the help of similarity restraints (SIMU, SADI) and rigid bond restraints (RIGU).<sup>[S8]</sup> The relative occupancies of the two alternative orientations of each group were refined to 0.60(2)/0.40(2) (benzyl) and 0.646(5)/0.354(5) (pmdta), respectively.

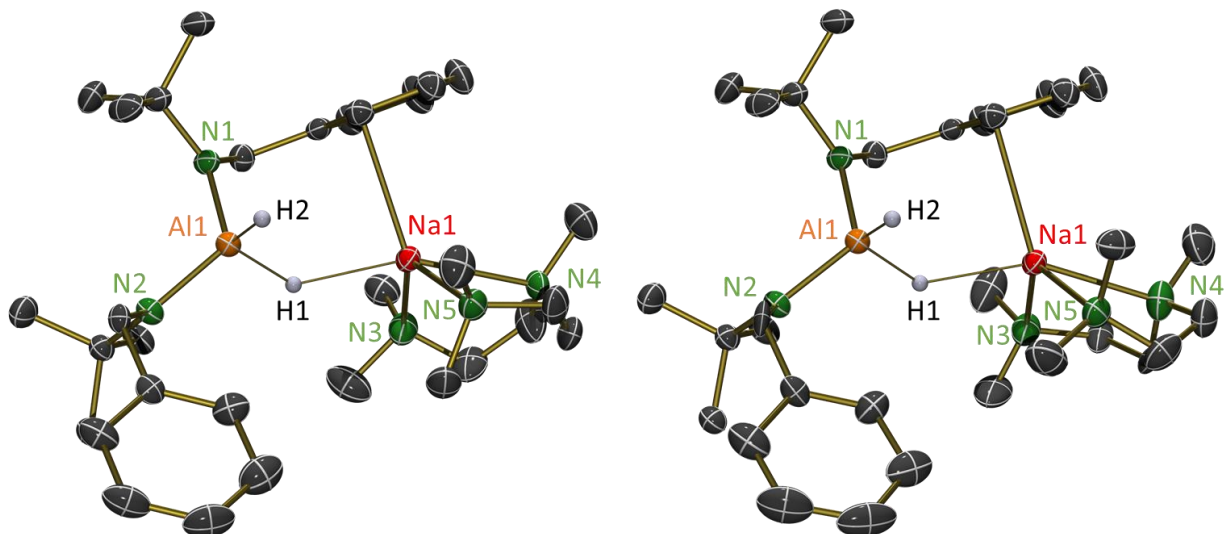


Figure S42: ORTEP-plot (50% probability) of  $\text{NaAlH}_2[\text{N}(\text{tBu})\text{CH}_2\text{Ph}]_2\cdot\text{PMDTA}$  (**3**). H atoms except for those bound to Al are omitted for clarity. Due to disorder, the different orientations of the amide and PMDTA are shown left and right respectively.

#### Structure determination of $\text{KAIH}_2[\text{N}(\text{tBu})\text{CH}_2\text{Ph}]_2\cdot18\text{-crown-6}$ (**4**)

A colorless crystal of  $[(18\text{-crown-6})\text{K(H)}_2\text{Al}(\text{tBuNCH}_2\text{C}_6\text{H}_5)_2]$  was embedded in inert perfluoropolyalkylether (viscosity 1800 cSt; ABCR GmbH) and mounted using a Hampton Research CryoLoop. The crystal was then flash cooled to 100.0(2) K in a nitrogen gas stream and kept at this temperature during the experiment. The crystal structure was measured on a SuperNova diffractometer with Atlas S2 detector using a CuK $\alpha$  microfocus source. The measured data was processed with the CrysAlisPro (v40.53) software package.<sup>[S4]</sup> Using Olex2,<sup>[S5]</sup> the structure was solved with the ShelXT<sup>[S6]</sup> structure solution program using Intrinsic Phasing and refined with the ShelXL<sup>[S7]</sup> refinement package using Least Squares Minimization. All non-hydrogen atoms were refined anisotropically. Most hydrogen atoms were placed in ideal positions and

refined as riding atoms with relative isotropic displacement parameters. The metal bound hydrides were observed from difference Fourier maps and refined.

Disorder of one benzyl group and of the whole K(18-crown-6) fragment was observed. The disorder was modeled with the help of similarity restraints (SIMU, SADI) and rigid bond restraints (RIGU).<sup>[S8]</sup> Additionally, a FLAT restraint was used for the aromatic ring of the less occupied orientation of the benzyl moiety. The relative occupancies of the two alternative orientations of the benzyl group were refined to 0.681(18) and 0.319(18), respectively. The disorder of the K(18-crown-6) fragment was more severe. While the potassium ion has two alternative positions with relative occupancies of 0.7986(14) and 0.2013(14), at least the 18-crown-6 ligand, which corresponds to the major potassium position, is additionally disordered (disorder within a disorder). Therefore, it was necessary to model the disorder of two sections of this 18-crown-6 as three alternative orientations. The related site occupancy factors are 0.460(3)/0.2013(14)/0.339(3) (section 1) and 0.455(3)/0.2013(14)/0.344(3) (section 2), respectively

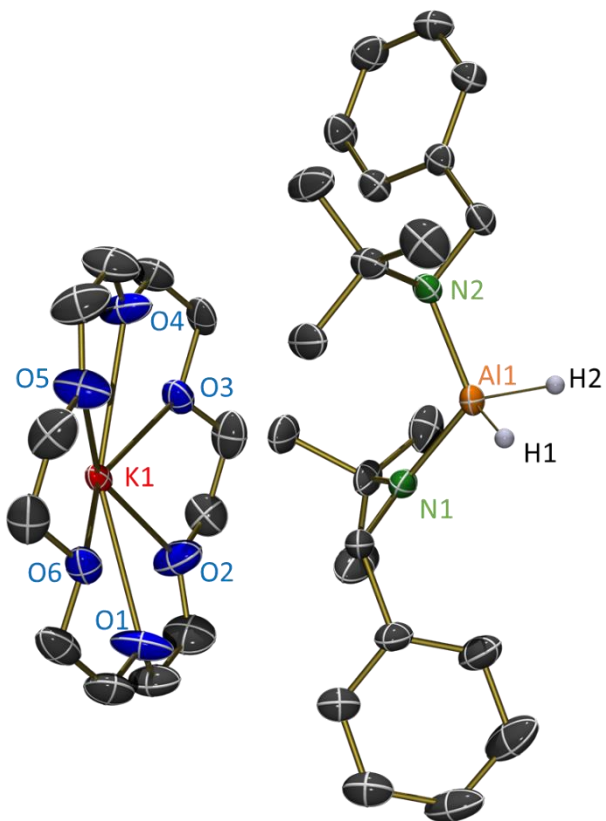


Figure S43: ORTEP-plot (50% probability) of  $\text{KAlH}_2[\text{N}(t\text{Bu})\text{CH}_2\text{Ph}]_2\cdot18\text{-crown-6}$  (**4**). H atoms except for those bound to Al are omitted for clarity. Disorder in the 18-crown-6 ligand and the phenyl ring of one amide omitted for clarity.

### Structure Determination of $\text{LiAlH}_2[\text{N}(t\text{Bu})\text{CH}_2t\text{Bu}]_2\cdot(\text{TMEDA})$ (5)

A colorless crystal of  $[(\text{tmeda})\text{Li}(\text{H})_2\text{Al}(t\text{BuNCH}_2t\text{Bu})_2]$  was embedded in inert perfluoropolyalkylether (viscosity 1800 cSt; ABCR GmbH) and mounted using a Hampton Research CryoLoop. The crystal was then flash cooled to 100.0(2) K in a nitrogen gas stream and kept at this temperature during the experiment. The crystal structure was measured on a SuperNova diffractometer with Atlas S2 detector using a  $\text{CuK}\alpha$  microfocus source. The measured data was processed with the CrysAlisPro (v40.67a) software package.<sup>[59]</sup> Using Olex2,<sup>[55]</sup> the structure was solved with the ShelXT<sup>[56]</sup> structure solution program using Intrinsic Phasing and refined with the ShelXL<sup>[57]</sup> refinement package using Least Squares Minimization. Most hydrogen atoms were placed in ideal positions and refined as riding atoms with relative isotropic displacement parameters. The metal bound hydrides were observed from difference Fourier maps and refined.

Disorder of one  $t\text{BuNCH}_2t\text{Bu}$  ligand was observed and modeled with the help of similarity restraints (SIMU, SADI) and rigid bond restraints (RIGU).<sup>[58]</sup> The relative occupancies of the two alternative orientations were refined to 0.787(2) and 0.213(2).

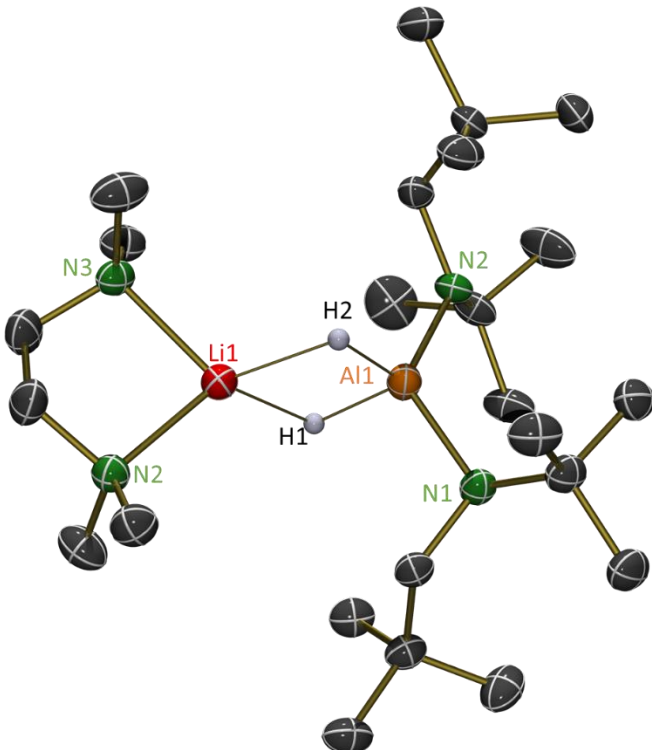


Figure S44: ORTEP-plot (50% probability) of  $\text{LiAlH}_2[\text{N}(t\text{Bu})\text{CH}_2t\text{Bu}]_2\cdot(\text{TMEDA})$  (5). H atoms except for those bound to Al are omitted for clarity. Disorder in one amide ligand omitted for clarity.

### Structure Determination of $\text{LiAl}[\text{N}(\text{Ph})\text{CH}_2\text{Ph}]_4\cdot(\text{THF})_4$ (6)

A colorless crystal of  $\text{LiAl}[\text{N}(\text{Ph})\text{CH}_2\text{Ph}]_4\cdot(\text{THF})_4$  was embedded in inert perfluoropolyalkylether (viscosity 1800 cSt; ABCR GmbH) and mounted using a Hampton Research CryoLoop. The crystal was then flash cooled to 100.0(2) K in a nitrogen gas stream and kept at this temperature during the experiment. The

crystal structure was measured on a SuperNova diffractometer with Atlas S2 detector using a CuK $\alpha$  microfocus source. The measured data was processed with the CrysAlisPro (v40.53) software package.<sup>[S4]</sup> Using Olex2,<sup>[S5]</sup> the structure was solved with the ShelXT<sup>[S6]</sup> structure solution program using Intrinsic Phasing and refined with the ShelXL<sup>[S7]</sup> refinement package using Least Squares Minimization. All hydrogen atoms were placed in ideal positions and refined as riding atoms with relative isotropic displacement parameters. The crystal under investigation suffered from non-merohedral twinning. The fractional contributions of the two twin domains were refined to 0.6944(17) and 0.3056(17).

Both, the lithium and the aluminum atom reside on a crystallographic mirror plane, while the thf and amide ligands are disordered about this symmetry element. The disorder was modeled with the help of similarity restraints (SIMU, SADI) and an additional FLAT restraint to keep the carbon atoms C34 – C39 of a phenyl group in-plane.

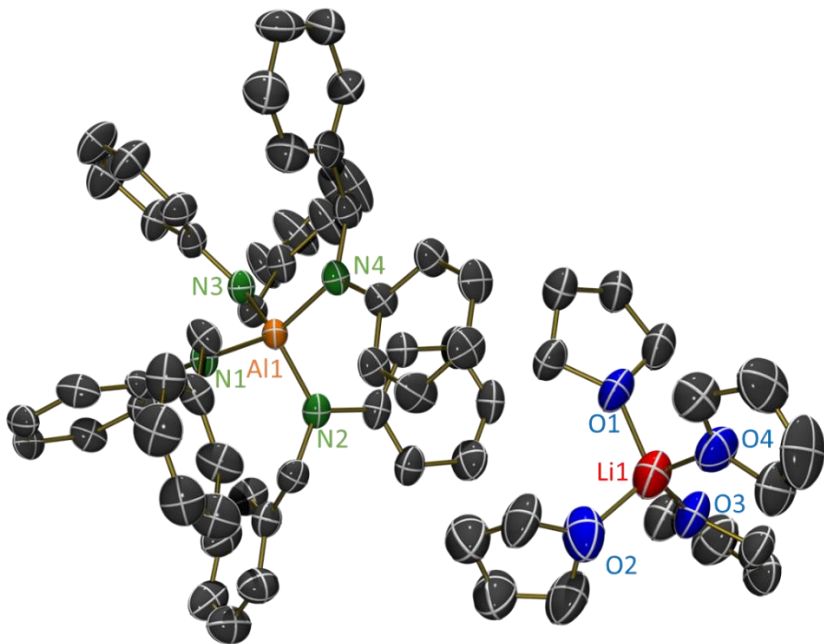


Figure S45: ORTEP-plot (50% probability) of LiAl[N(Ph)CH<sub>2</sub>Ph]<sub>4</sub>·(THF)<sub>4</sub> (**6**). H are omitted for clarity.

### Structure Determination of **7**

A colorless crystal of **7** was embedded in inert perfluoropolyalkylether (viscosity 1800 cSt; ABCR GmbH) and mounted using a Hampton Research CryoLoop. The crystal was then flash cooled to 100.0(1) K in a nitrogen gas stream and kept at this temperature during the experiment. The crystal structure was measured on a SuperNova diffractometer with Atlas S2 detector using a CuK $\alpha$  microfocus source. The measured data was processed with the CrysAlisPro (v39.46) software package.<sup>[S4]</sup> Using Olex2<sup>[S5]</sup>, the structure was solved with the ShelXT<sup>[S6]</sup> structure solution program using Intrinsic Phasing and refined with the ShelXL<sup>[S7]</sup> refinement package using Least Squares minimization. Except of the NH hydrogen atom, all hydrogen atoms were placed in ideal positions and refined as riding atoms with relative isotropic displacement parameters. The position of the NH hydrogen atom was observed from difference Fourier

maps and refined. The crystal shows disorder concerning coordination of substrate/product (imine/amine). The disorder was refined over two positions (ratio ~ 50:50).

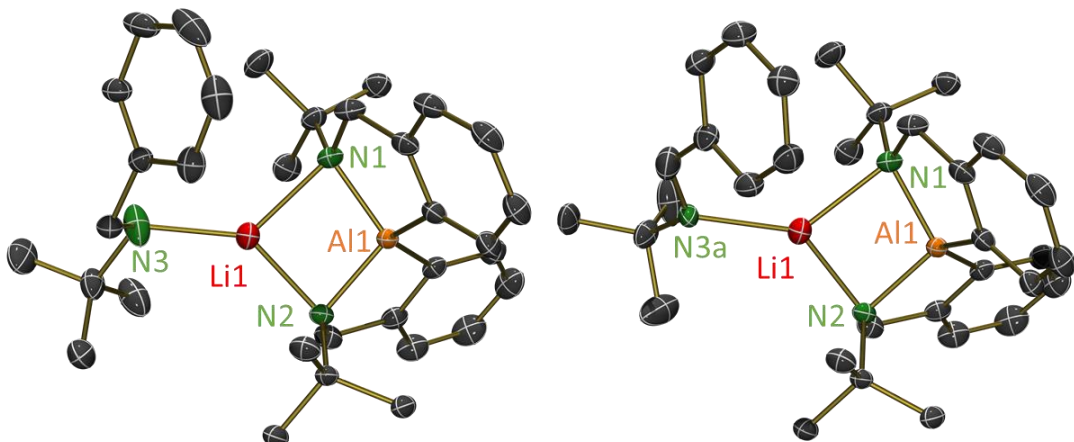


Figure S46: ORTEP-plot (50% probability) of 7. H atoms except for those bound to Al are omitted for clarity. Due to disorder, the coordination of imine and amine are shown left and right respectively.

### Structure determination of 8

A colorless crystal of  $[\text{Li}(\text{thf})_4][\text{Al}(t\text{BuNCH}_2\text{C}_6\text{H}_4)_2]$  was embedded in inert perfluoropolyalkylether (viscosity 1800 cSt; ABCR GmbH) and mounted using a Hampton Research CryoLoop. The crystal was then flash cooled to 100.0(3) K in a nitrogen gas stream and kept at this temperature during the experiment. The crystal structure was measured on a SuperNova diffractometer with Atlas S2 detector using a CuK $\alpha$  microfocus source. The measured data was processed with the CrysAlisPro (v40.53) software package.<sup>[S4]</sup> Using Olex2,<sup>[S5]</sup> the structure was solved with the ShelXT<sup>[S6]</sup> structure solution program using Intrinsic Phasing and refined with the ShelXL<sup>[S7]</sup> refinement package using Least Squares Minimization. All non-hydrogen atoms were refined anisotropically. All hydrogen atoms were placed in ideal positions and refined as riding atoms with relative isotropic displacement parameters. The crystal under investigation suffered from non-merohedral twinning. The fractional contributions of the two twin domains were refined to 0.6321(9) and 0.3679(9).

Additionally, disorder of one thf ligand was observed and modeled with the help of similarity restraints (SIMU, SADI). The relative occupancies of its two alternative orientations were refined to 0.79(2) and 0.21(2), respectively.

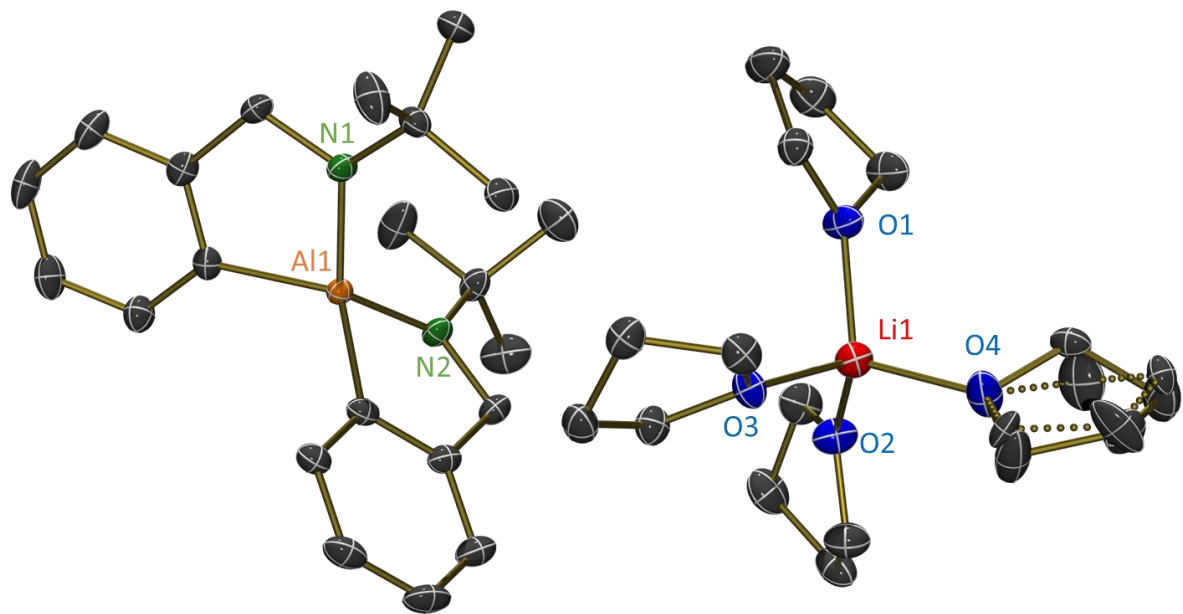


Figure S47: ORTEP-plot (50% probability) of **8**. H atoms are omitted for clarity.

Table S1: Crystal data.

Identification code (CCDC)	<b>1</b> (2024356)	<b>2</b> (2024357)	<b>3</b> (2024358)
Empirical formula	C <sub>49</sub> H <sub>81</sub> AlLiN <sub>3</sub> O <sub>4</sub>	C <sub>34</sub> H <sub>66</sub> AlN <sub>6</sub> Na	C <sub>31</sub> H <sub>57</sub> AlN <sub>5</sub> Na
Formula weight	810.08	608.89	549.78
Temperature/K	100.0(1)	100.00(11)	100.0(2)
Crystal system	orthorhombic	monoclinic	orthorhombic
Space group	Aea2	P2 <sub>1</sub> /n	Pbca
a/Å	28.8649(2)	11.4625(2)	13.0409(2)
b/Å	19.2621(2)	16.9597(2)	17.1247(3)
c/Å	17.41050(10)	20.1935(3)	30.7112(4)
α/°	90	90	90
β/°	90	95.190(2)	90
γ/°	90	90	90
Volume/Å <sup>3</sup>	9680.21(13)	3909.53(10)	6858.45(19)
Z	8	4	8
ρ <sub>calc</sub> g/cm <sup>3</sup>	1.112	1.034	1.065
μ/mm <sup>-1</sup>	0.696	0.767	0.822
F(000)	3552.0	1344.0	2416.0
Crystal size/mm <sup>3</sup>	0.503 × 0.247 × 0.202	0.399 × 0.294 × 0.199	0.206 × 0.111 × 0.083
Radiation	Cu Kα (λ = 1.54184)	Cu Kα (λ = 1.54184)	Cu Kα (λ = 1.54184)
2θ range for data collection/°	6.124 to 145.608	8.554 to 144.766	8.896 to 145.426
Index ranges	-35 ≤ h ≤ 35, -21 ≤ k ≤ 23, -17 ≤ l ≤ 21	-12 ≤ h ≤ 14, -20 ≤ k ≤ 20, -17 ≤ l ≤ 24	-15 ≤ h ≤ 14, -20 ≤ k ≤ 20, -37 ≤ l ≤ 31
Reflections collected	43938	21932	15730
Independent reflections	8559 [R <sub>int</sub> = 0.0257, R <sub>sigma</sub> = 0.0192]	7549 [R <sub>int</sub> = 0.0273, R <sub>sigma</sub> = 0.0253]	6630 [R <sub>int</sub> = 0.0313, R <sub>sigma</sub> = 0.0342]
Data/restraints/parameters	8559/1/536	7549/9/420	6630/399/522
Goodness-of-fit on F <sup>2</sup>	1.027	1.086	1.022
Final R indexes [I>=2σ (I)]	R <sub>1</sub> = 0.0274, wR <sub>2</sub> = 0.0697	R <sub>1</sub> = 0.0591, wR <sub>2</sub> = 0.1557	R <sub>1</sub> = 0.0505, wR <sub>2</sub> = 0.1334
Final R indexes [all data]	R <sub>1</sub> = 0.0281, wR <sub>2</sub> = 0.0705	R <sub>1</sub> = 0.0653, wR <sub>2</sub> = 0.1614	R <sub>1</sub> = 0.0608, wR <sub>2</sub> = 0.1448
Largest diff. peak/hole / e Å <sup>-3</sup>	0.20/-0.18	0.54/-0.28	0.46/-0.34

Table S1: Continued.

Identification code (CCDC)	<b>4</b> (2024359)	<b>5</b> (2024360)	<b>6</b> (2024361)
Empirical formula	C <sub>34</sub> H <sub>58</sub> AlKN <sub>2</sub> O <sub>6</sub>	C <sub>24</sub> H <sub>58</sub> AlLiN <sub>4</sub>	C <sub>68</sub> H <sub>80</sub> AlLiN <sub>4</sub> O <sub>4</sub>
Formula weight	656.90	436.66	1051.28
Temperature/K	100.0(2)	100.0(1)	100.0(2)
Crystal system	orthorhombic	monoclinic	monoclinic
Space group	Pbca	P2 <sub>1</sub> /c	P2 <sub>1</sub> /m
a/Å	10.4344(3)	11.7729(3)	11.7199(6)
b/Å	16.9623(5)	11.0678(3)	19.4526(9)
c/Å	42.5886(9)	22.8213(6)	12.8802(8)
α/°	90	90	90
β/°	90	92.037(2)	95.899(5)
γ/°	90	90	90
Volume/Å <sup>3</sup>	7537.8(3)	2971.74(13)	2920.9(3)
Z	8	4	2
ρ <sub>calc</sub> g/cm <sup>3</sup>	1.158	0.976	1.195
μ/mm <sup>-1</sup>	1.792	0.688	0.705
F(000)	2848.0	984.0	1128.0
Crystal size/mm <sup>3</sup>	0.194 × 0.094 × 0.075	0.32 × 0.171 × 0.143	0.168 × 0.159 × 0.061
Radiation	Cu Kα (λ = 1.54184)	Cu Kα (λ = 1.54184)	Cu Kα (λ = 1.54184)
2θ range for data collection/°	8.304 to 145.424	7.514 to 145.692	7.584 to 144.734
Index ranges	-6 ≤ h ≤ 12, -18 ≤ k ≤ 20, -52 ≤ l ≤ 36	-14 ≤ h ≤ 13, -13 ≤ k ≤ 13, -26 ≤ l ≤ 28	-14 ≤ h ≤ 14, -23 ≤ k ≤ 23, -15 ≤ l ≤ 15
Reflections collected	17113	22800	9908
Independent reflections	7273 [R <sub>int</sub> = 0.0287, R <sub>sigma</sub> = 0.0331]	5811 [R <sub>int</sub> = 0.0358, R <sub>sigma</sub> = 0.0262]	9908 [R <sub>int</sub> = ?, R <sub>sigma</sub> = 0.0251]
Data/restraints/parameters	7273/3216/679	5811/159/392	9908/2597/695
Goodness-of-fit on F <sup>2</sup>	1.020	1.028	1.043
Final R indexes [I>=2σ (I)]	R <sub>1</sub> = 0.0574, wR <sub>2</sub> = 0.1386	R <sub>1</sub> = 0.0446, wR <sub>2</sub> = 0.1162	R <sub>1</sub> = 0.0848, wR <sub>2</sub> = 0.2308
Final R indexes [all data]	R <sub>1</sub> = 0.0691, wR <sub>2</sub> = 0.1477	R <sub>1</sub> = 0.0492, wR <sub>2</sub> = 0.1215	R <sub>1</sub> = 0.1004, wR <sub>2</sub> = 0.2388
Largest diff. peak/hole / e Å <sup>-3</sup>	0.64/-0.39	0.60/-0.73	0.37/-0.36

Table S1: Continued.

Identification code (CCDC)	<b>7</b> (2024362)	<b>8</b> (2024363)
Empirical formula	C <sub>33</sub> H <sub>46</sub> AlLiN <sub>3</sub>	C <sub>38</sub> H <sub>62</sub> AlLiN <sub>2</sub> O <sub>4</sub>
Formula weight	518.66	644.81
Temperature/K	100	100.0(3)
Crystal system	Monoclinic	monoclinic
Space group	P2 <sub>1</sub> /n	P2 <sub>1</sub>
a/Å	10.59708(6)	10.7366(11)
b/Å	17.20443(9)	16.7030(13)
c/Å	16.60664(10)	11.1891(11)
α/°	90	90
β/°	90.7848(6)	109.155(11)
γ/°	90	90
Volume/Å <sup>3</sup>	3027.39(3)	1895.5(3)
Z	4	2
ρ <sub>calc</sub> g/cm <sup>3</sup>	1.138	1.130
μ/mm <sup>-1</sup>	0.759	0.764
F(000)	1124.0	704.0
Crystal size/mm <sup>3</sup>	0.576 × 0.435 × 0.353	0.171 × 0.147 × 0.083
Radiation	CuKα (λ = 1.54184)	Cu Kα (λ = 1.54184)
2θ range for data collection/°	7.4 to 145.868	8.366 to 145.286
Index ranges	-13 ≤ h ≤ 13, -21 ≤ k ≤ 21, -20 ≤ l ≤ 20	-13 ≤ h ≤ 13, -20 ≤ k ≤ 20, -13 ≤ l ≤ 13
Reflections collected	55738	13786
Independent reflections	5994 [R <sub>int</sub> = 0.0369, R <sub>sigma</sub> = 0.0148]	13786 [R <sub>int</sub> = ?, R <sub>sigma</sub> = 0.0222]
Data/restraints/parameters	5994/0/459	13786/230/459
Goodness-of-fit on F <sup>2</sup>	1.045	1.019
Final R indexes [I>=2σ (I)]	R <sub>1</sub> = 0.0352, wR <sub>2</sub> = 0.0920	R <sub>1</sub> = 0.0412, wR <sub>2</sub> = 0.1081
Final R indexes [all data]	R <sub>1</sub> = 0.0367, wR <sub>2</sub> = 0.0932	R <sub>1</sub> = 0.0431, wR <sub>2</sub> = 0.1092
Largest diff. peak/hole / e Å <sup>-3</sup>	0.24/-0.25	0.28/-0.28

## Calculations

### Computational Details

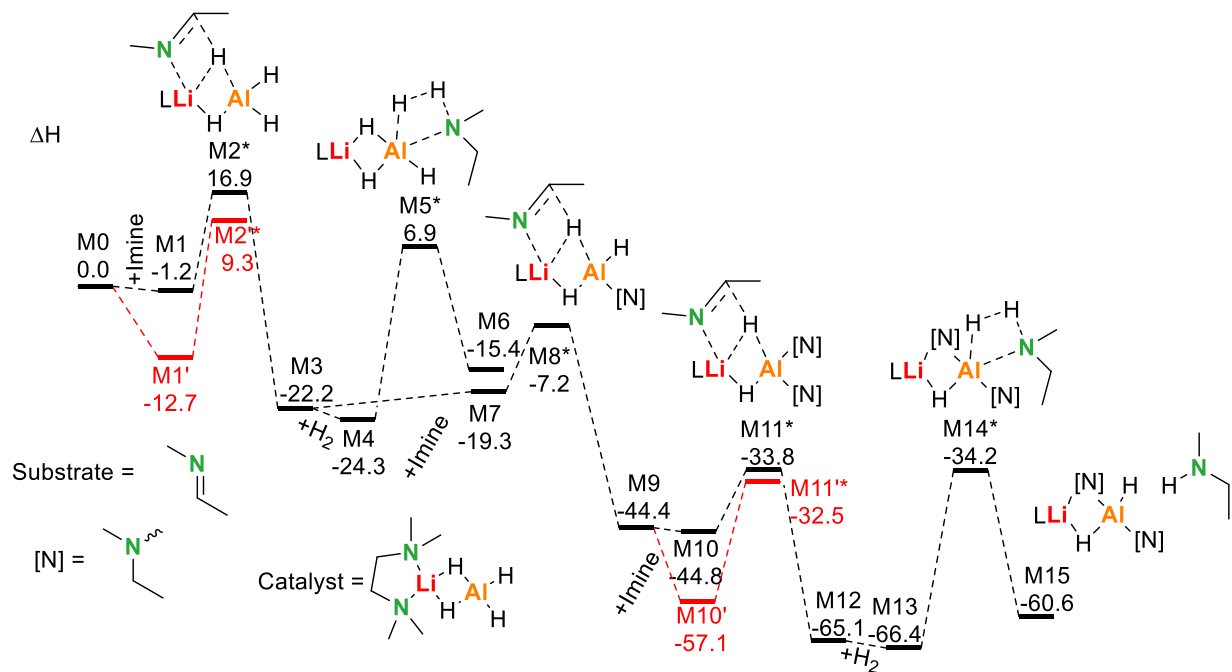
All calculations were carried out using Gaussian 16A.<sup>[S10]</sup> All structures were fully optimized on a B3PW91/6-31+G\*\* level of theory.<sup>[S11-S15]</sup> Harmonic frequency calculations were carried out on the same level of theory to characterize the structures as minima (NIMAG=0) or transition states (NIMAG=1). For higher accuracy, single point energies were determined on B3PW91/6-311++G\*\*//6-31+G\*\* level of theory. Solvent effects were modeled via polarizable continuum model (PCM) simulating THF ( $\epsilon = 7.4257$ ).<sup>[S16]</sup> In all energy profiles  $\Delta H$  is given in kcal/mol.

### Effect of solvation

Initial calculations were carried out using a simple model system with imine MeC(H)=NMe and LiAlH<sub>4</sub>·TMEDA as catalyst. This allowed for the identification of stationary point geometries and the evaluation of solvent effects. TMEDA was chosen as explicit solvent as experimental results found that it does not have a negative effect on catalytic performance. It also provides a more realistic solvation effect than continuum based solvent models like PCM.

Imine to amide reduction was found to have activation barriers of **M1-M2\***: 18.1, **M7-M8\***: 12.1, **M10-M11\***: 11.0 kcal/mol. Imine insertion into the metal hydride bond becomes easier with an increasing number of amide ligands present. Four imine insertions, however, are not possible. The rate determining step is generally the hydrogenolysis step with **M4-M5\***: 31.2 and **M13-M14\***: 32.2 kcal/mol. These energies are slightly too high for a reaction at 85 °C. This may be partially attributed to the fact that imines with alkyl substituents on C and N are difficult to convert.

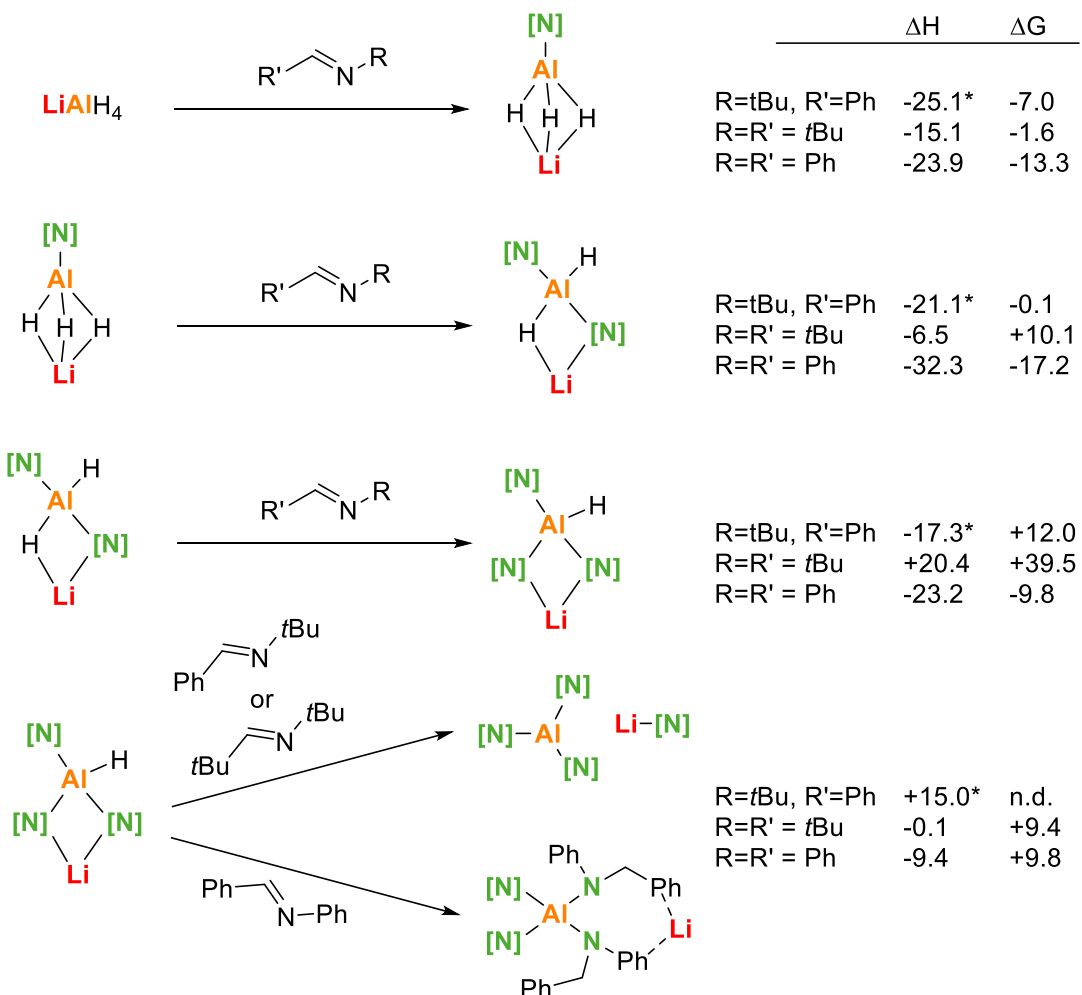
Removal of TMEDA (energy levels **M1'-M2'\*** and **M10'-M11'\*** marked in red) shows an increase for the imine insertion barriers. Without the explicit solvent molecule coordinated to lithium, the activation energies for these two steps increased from 18.1 to 20.0 and from 11.0 to 24.6 kcal/mol, respectively. This is an effective increase in activation barrier of 18 and 55 %. It shows that, for strongly ionic species such as LiAlH<sub>4</sub>, it is very important to model solvation explicitly with solvent molecules (or in this case a polar imine). For further calculations (Mechanisms A-D) imine PhC(H)=NtBu was chosen as both substrate and coordinated solvent molecule (the majority of catalytic experiments were carried out in neat imine without additional solvent).



Scheme S1: Energy profile (B3PW91/6-311++G\*\*(PCM=THF)//6-31+G\*\*) for the hydrogenation of MeC(H)=NMe with the catalyst LiAlH4·TMEDA ( $L = \text{TMEDA}$ ,  $[N] = \text{N}(\text{Me})\text{Et}$ ). The energy levels in red (**M1'**, **M2''\***, **M10'** and **M11''\***) represent optimized structures without the TMEDA ligand.

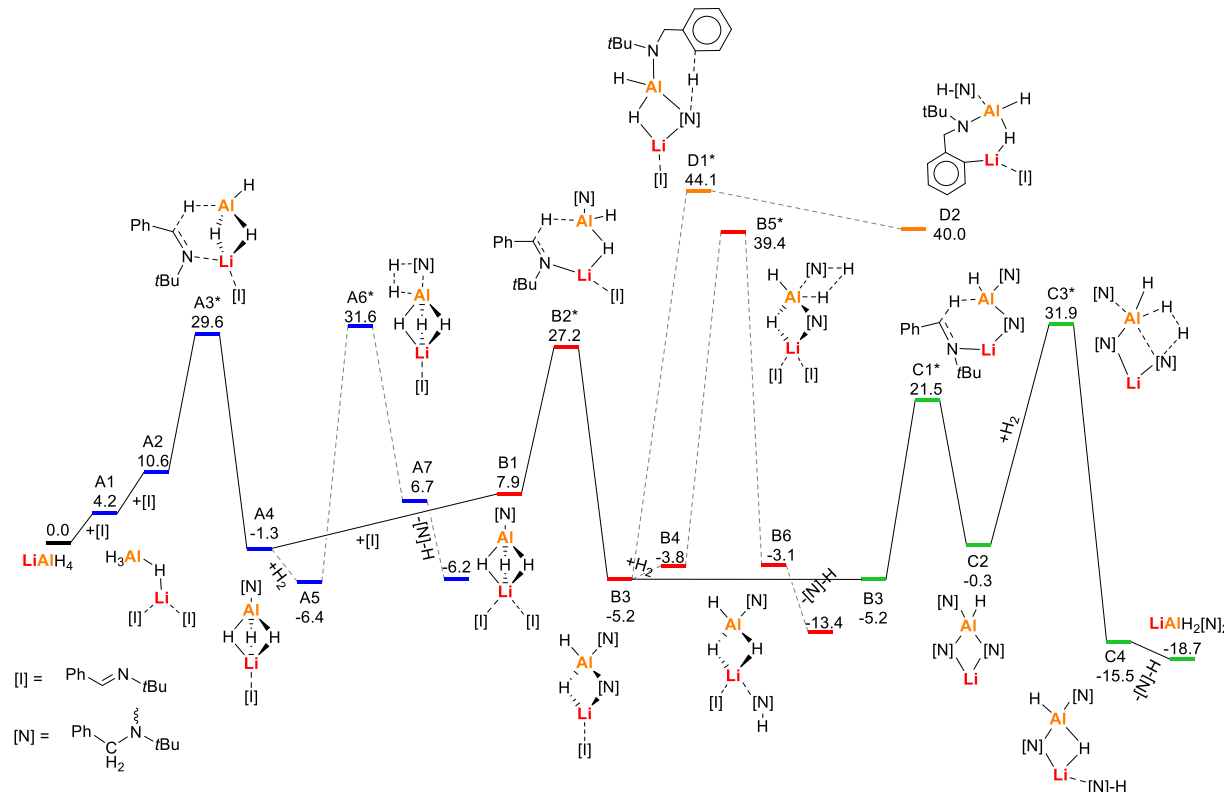
## Thermodynamics of sequential imine insertion in $\text{LiAlH}_4$

The reaction energies for insertion of different imines in the Al-H bonds of  $\text{LiAlH}_4$  have been calculated. It can be concluded that  $t\text{BuC(H)}=\text{N}t\text{Bu}$  can realistically insert twice and  $\text{PhC(H)}=\text{N}t\text{Bu}$  three times. More insertions are endothermic and endergonic. After four imine insertions the complex dissociates in Al amide and Li amide species. The highly activated imine,  $\text{PhC(H)}=\text{NPh}$ , can insert four times and the resulting complex is stable due to  $\text{Ph}\cdots\text{Li}$  interactions.

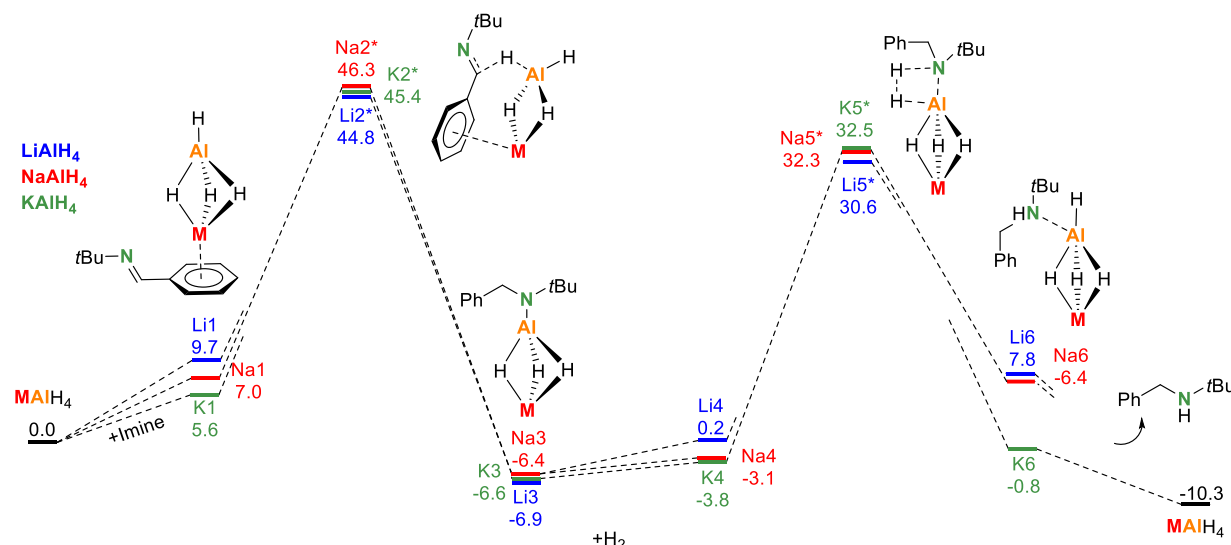


Scheme S2: Reaction energy for the reaction of  $\text{LiAlH}_4$  with one, two, three, and four equivalents of  $\text{PhC(H)}=\text{N}t\text{Bu}$ ,  $t\text{BuC(H)}=\text{N}t\text{Bu}$ , and  $\text{Ph(H)C=NPh}$ .  $\Delta H$  and  $\Delta G$  ( $85^\circ\text{C}$ , 6 bar, PCM correction for the polar solvent THF) given in kcal/mol. \*For  $\text{PhC(H)}=\text{N}t\text{Bu}$  only  $\Delta E$  was calculated instead of  $\Delta H$ .<sup>[S17]</sup>

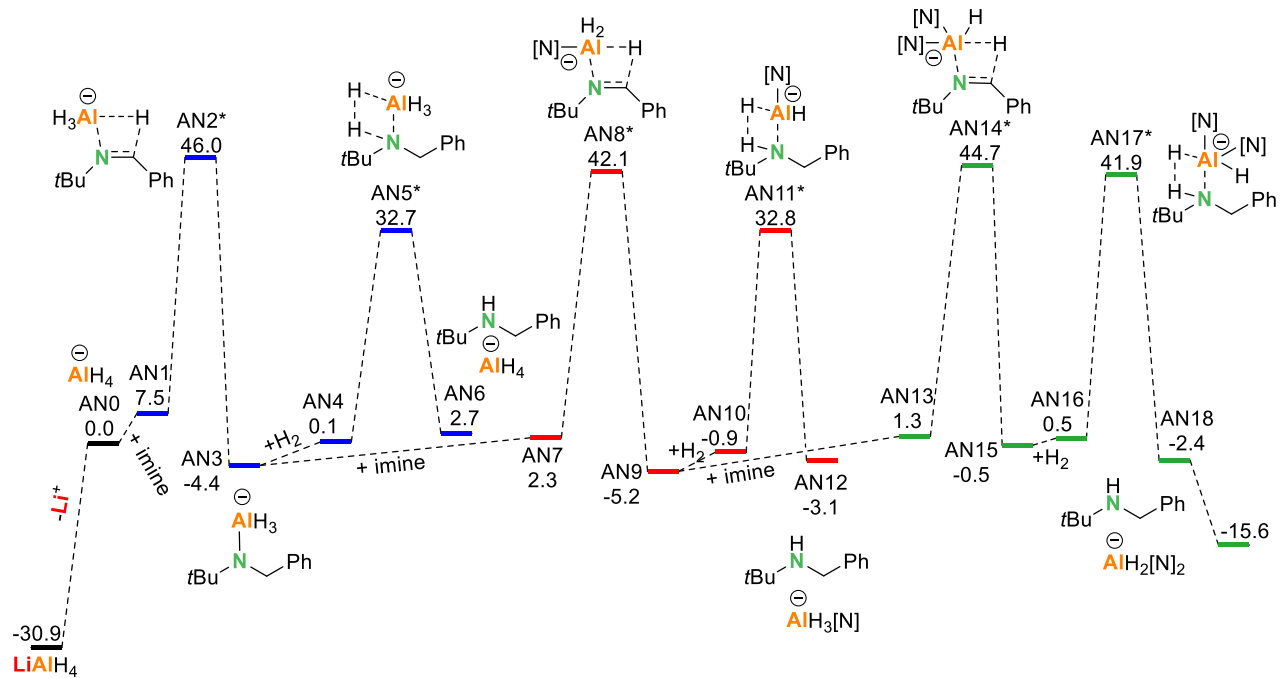
### Energy profiles with DG values (kcal/mol)



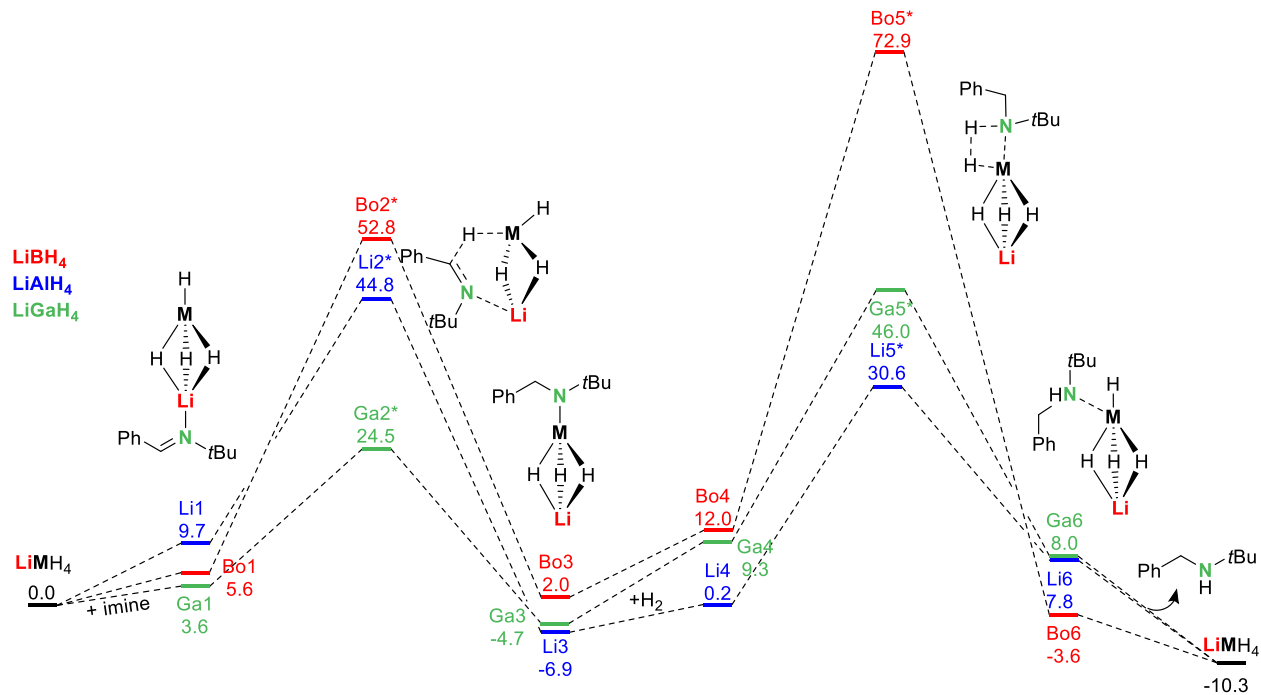
Scheme S3: Full energy profile ( $\Delta G$  (358 K, 6 bar)) for the hydrogenation of  $\text{PhC}(\text{H})=\text{NtBu}$  with  $\text{LiAlH}_4$  using the imine as explicit solvent (B3PW91/6-311++G\*\* (PCM=THF)//6-31+G\*\*). Pathways A (blue) and B (red) show the formation of the active catalyst:  $\text{LiAlH}_2[\text{N}]_2$  (B3). Pathway C (green) represents the catalytic cycle for **B3**. is the catalytic cycle. Path D (grey) shows a pathway for catalyst decomposition by ortho-metallation. The most likely intermediates are connected by solid lines.



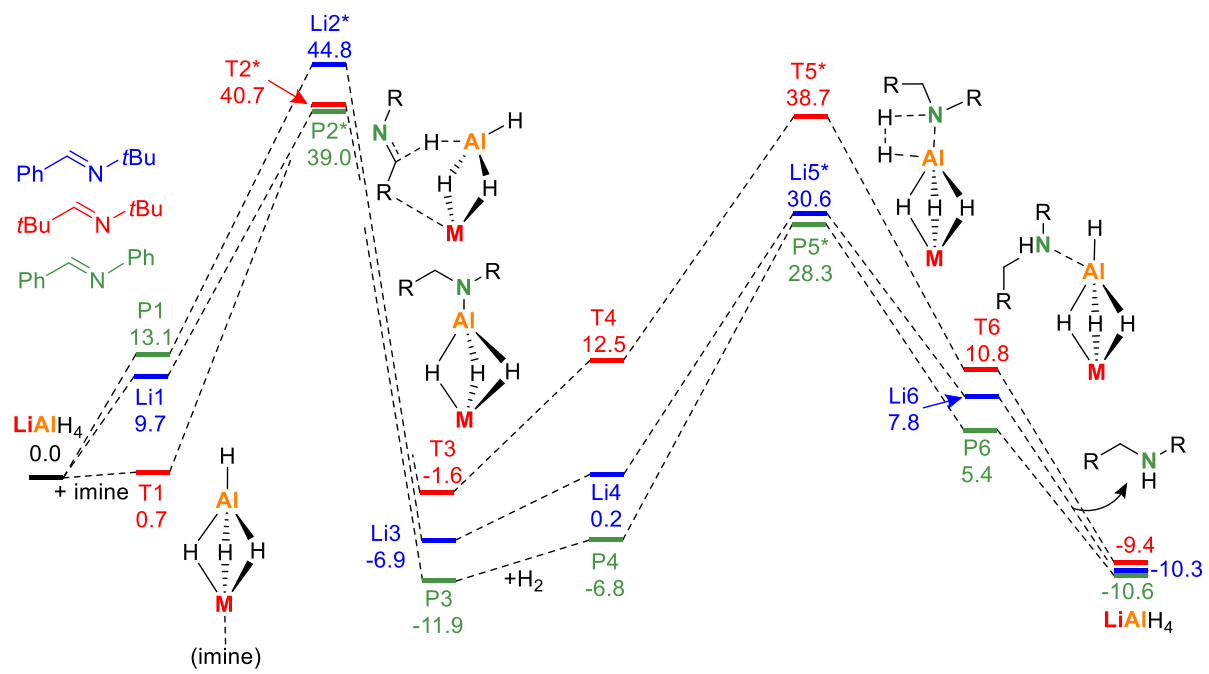
Scheme S4: Comparison of the metal influence on hydrogenation of imines with  $\text{MAIH}_4$  catalysts ( $M = \text{Li}, \text{Na}, \text{K}$ ) ( $\Delta G$  (358 K, 6 bar)); B3PW91/6-311++G\*\* (PCM=THF)//6-31+G\*\*.



Scheme S5: Full energy profile ( $\Delta G$  (358 K, 6 bar)) for the hydrogenation of  $\text{PhC}(\text{H})=\text{NtBu}$  with the anion  $\text{AlH}_4^-$  (B3PW91/6-311++G\*\* (PCM=THF)//6-31+G\*\*).



Scheme S6: Comparison of the (half)metal influence on hydrogenation of imines with  $\text{LiMH}_4$  catalysts ( $\text{M} = \text{B}, \text{Al}, \text{Ga}$ ); ( $\Delta G$  (358 K, 6 bar)) B3PW91/6-311++G\*\* (PCM=THF)//6-31+G\*\*.



Scheme S7: Comparison of imine substituent effects in hydrogenation with a  $\text{LiAlH}_4$  catalyst; ( $\Delta G$  (358 K, 6 bar)) B3PW91/6-311++G\*\* (PCM=THF)//6-31+G\*\*.







































## References

- [S1] S.-N. Trzaska, Alkalimetallbortetrahydride und -Aluminiumtetrahydride, Universität Hamburg, **2008**.
- [S2] N. Momiyama, H. Nishimoto, M. Terada, *Org. Lett.* **2011**, 13, 2126–2129.
- [S3] X. Cattoën, S. Solé, C. Pradel, H. Gornitzka, K. Miqueu, D. Bourissou, G. Bertrand, *J. Org. Chem.* **2003**, 68, 911–914.
- [S4] Rigaku Oxford Diffraction, **2018**, CrysAlisPro Software system, version 1.171.39.46, Rigaku Corporation, Oxford, UK.
- [S5] O. V. Dolomanov, L. J. Bourhis, R.J. Gildea, J. A. K. Howard and H. Puschmann, *J. Appl. Cryst.*, **2009**, 42, 339–341.
- [S6] G. M. Sheldrick, *Acta Cryst. A*, **2015**, 71, 3–8.
- [S7] G. M. Sheldrick, *Acta Cryst.* **2008**, A64, 112–122.
- [S8] A. Thorn, B. Dittrich and G. M. Sheldrick, *Acta Cryst. A*, **2012**, 68, 448–451.
- [S9] Rigaku Oxford Diffraction, **2019**, CrysAlisPro Software system, version 1.171.40.67a, Rigaku Corporation, Oxford, UK.
- [S10] M. J. Frisch, G. W. Trucks, H. B. Schlegel, G. E. Scuseria, M. A. Robb, J. R. Cheeseman, G. Scalmani, V. Barone, G. A. Petersson, H. Nakatsuji, X. Li, M. Caricato, A. V. Marenich, J. Bloino, B. G. Janesko, R. Gomperts, B. Mennucci, H. P. Hratchian, J. V. Ortiz, A. F. Izmaylov, J. L. Sonnenberg, D. Williams-Young, F. Ding, F. Lipparini, F. Egidi, J. Goings, B. Peng, A. Petrone, T. Henderson, D. Ranasinghe, V. G. Zakrzewski, J. Gao, N. Rega, G. Zheng, W. Liang, M. Hada, M. Ehara, K. Toyota, R. Fukuda, J. Hasegawa, M. Ishida, T. Nakajima, Y. Honda, O. Kitao, H. Nakai, T. Vreven, K. Throssell, J. A. Montgomery, J. E. Peralta, F. Ogliaro, M. J. Bearpark, J. J. Heyd, E. N. Brothers, K. N. Kudin, V. N. Staroverov, T. A. Keith, R. Kobayashi, J. Normand, K. Raghavachari, A. P. Rendell, J. C. Burant, S. S. Iyengar, J. Tomasi, M. Cossi, J. M. Millam, M. Klene, C. Adamo, R. Cammi, J. W. Ochterski, R. L. Martin, K. Morokuma, O. Farkas, J. B. Foresman, D. J. Fox, Gaussian 16 Rev. A.03, Wallingford CT, **2016**.
- [S11] A. D. Becke, *J. Chem. Phys.* **1993**, 98, 1372–1377.
- [S12] J. P. Perdew, Electronic Structure of Solids, Akademie Verlang, Berlin, **1991**.
- [S13] W. J. Hehre, L. Radom, P. v. R. Schleyer, J. A. Pople, Ab Initio Molecular Orbital Theory, John Wiley, New York, **1986**.
- [S14] R. C. Binning, L. A. Curtiss, *J. Comput. Chem.* **1990**, 11, 1206–1216.
- [S15] T. Clark, J. Chandrasekhar, G. W. Spitznagel, P. v. R. Schleyer, *J. Comp. Chem.* **1983**, 4, 294–301.
- [S16] G. Scalmani, M. J. Frisch, *J. Chem. Phys.* **2010**, 132, 114110-1–16.
- [S17] H. Elsen, F. Christian, G. Ballmann, S. Harder, *Angew. Chemie - Int. Ed.* **2018**, 57, 7156–7160.